A Comparison of Southern Ocean Air–Sea Buoyancy Flux from an Ocean State Estimate with Five Other Products

IVANA CEROVEČKI, LYNNE D. TALLEY, AND MATTHEW R. MAZLOFF

Climate, Atmospheric Science and Physical Oceanography, Scripps Institution of Oceanography, University of California, San Diego, La Jolla, California

(Manuscript received 18 May 2010, in final form 31 May 2011)

ABSTRACT

The authors have intercompared the following six surface buoyancy flux estimates, averaged over the years 2005–07: two reanalyses [the recent ECMWF reanalysis (ERA-Interim; hereafter ERA), and the National Centers for Environmental Prediction (NCEP)–NCAR reanalysis 1 (hereafter NCEP1)], two recent flux products developed as an improvement of NCEP1 [the flux product by Large and Yeager and the Southern Ocean State Estimate (SOSE)], and two ad hoc air–sea flux estimates that are obtained by combining the NCEP1 or ERA net radiative fluxes with turbulent flux estimates using the Coupled Ocean–Atmosphere Response Experiment (COARE) 3.0 bulk formulas with NCEP1 or ERA input variables.

The accuracy of SOSE adjustments of NCEP1 atmospheric fields (which SOSE uses as an initial guess and a constraint) was assessed by verification that SOSE reduces the biases in the NCEP1 fluxes as diagnosed by the Working Group on Air–Sea Fluxes (Taylor), suggesting that oceanic observations may be a valuable constraint to improve atmospheric variables.

Compared with NCEP1, both SOSE and Large and Yeager increase the net ocean heat loss in high latitudes, decrease ocean heat loss in the subtropical Indian Ocean, decrease net evaporation in the subtropics, and decrease net precipitation in polar latitudes. The large-scale pattern of SOSE and Large and Yeager turbulent heat flux adjustment is similar, but the magnitude of SOSE adjustments is significantly larger. Their radiative heat flux adjustments patterns differ. Turbulent heat fluxes determined by combining COARE bulk formulas with NCEP1 or ERA should not be combined with unmodified NCEP1 or ERA radiative fluxes as the net ocean heat gain poleward of 25°S becomes unrealistically large. The other surface flux products (i.e., NCEP1, ERA, Large and Yeager, and SOSE) balance more closely.

Overall, the statistical estimates of the differences between the various air–sea heat flux products tend to be largest in regions with strong ocean mesoscale activity such as the Antarctic Circumpolar Current and the western boundary currents.

1. Introduction and outline

The Southern Ocean (SO) plays a fundamental role in setting the global climate, making detailed understanding of air–sea buoyancy fluxes in the region indispensable for climate modeling and prediction. However, the sparseness of both conventional and remotely sensed observations causes the availability and accuracy of air–sea buoyancy flux estimates to be especially poor in this region (Josey et al. 1999; Taylor 2000; Kubota et al. 2003; Dong et al. 2007; Gulev et al. 2007; M. Bourassa et al. 2011, personal communication). This situation decreases the quality of meteorological state variables estimated by numerical weather prediction (NWP) models and degrades the accuracy of bulk formulas, which are difficult to test and tune in a data-sparse region with such extreme conditions, high spatial variability, and large seasonal cycle.

Accurate estimates of ocean surface flux components with high spatial and temporal resolution are necessary not only for analysis of high-frequency events, but also for modeling and analysis of longer time scales, including climate processes. This is especially true for the high southern latitudes, where the temporal covariances between the fundamental atmospheric and oceanic variables are strong (Simmonds and Dix 1989; Gulev 1997)

Corresponding author address: Ivana Cerovečki, Scripps Institution of Oceanography, University of California, San Diego, La Jolla, CA 92093.
E-mail: icerovecki@ucsd.edu

DOI: 10.1175/2011JCLI3858.1

and nonlinearity in the equation of state is important (Moore and Renfrew 2002). Unfortunately, the presently available surface flux estimates do not provide the needed accuracy and resolution in any region (for details and review see, e.g., Taylor 2000; Curry et al. 2004; Röske 2006; Large and Yeager 2009, hereafter referred to as LY09). This long-standing problem motivated the formation of a Joint Scientific Committee/Scientific Committee for Oceanic Research (JSC/SCOR Working Group on Air–Sea Fluxes (WGASF) in 1997, whose task was to catalog the available surface flux datasets, evaluate the strengths and weaknesses of the existing flux products, and give an overview of the problem of estimating fluxes (Gulev 2003). The final report (Taylor 2000, hereafter WGASF) concluded that, at the time of the report, ''all existing flux estimates have deficiencies.'' Since the time of the WGASF report, a number of new contemporary global reanalyses have been developed as follows: the Japanese 25-yr Reanalysis Project (JRA-25), 1979–present; the European Centre for Medium-Range Weather Forecasts' (ECMWF) ''interim'' Reanalysis (ERA-Interim), 1989–present; the National Aeronautics and Space Administration (NASA) Modern Era Retrospective-Analysis for Research and Applications (MERRA), 1979–present; and the new National Centers for Environmental Prediction (NCEP) Climate Forecast System Reanalysis (CFSR), 1979–present. Even more are on the horizon, including JRA-55 and ERA-75.

We here make use of the ERA-Interim (hereafter ERA) (Simmons et al. 2006), the NCEP–National Center for Atmospheric Research (NCAR) reanalysis 1 (hereafter NCEP1) (Kalnay et al. 1996), the recent LY09 heat flux product, and a new air–sea buoyancy flux estimate diagnosed from the Southern Ocean State Estimate (SOSE) by Mazloff et al. (2010). The goal of this paper is to present the SOSE air–sea buoyancy flux estimate and to compare it with five other air–sea buoyancy flux products in the ice-free regions of the Southern Ocean for the years 2005–07, the 3 yr for which SOSE is available. Ours is the first such comparison. The SOSE air–sea buoyancy flux fields are of particular interest for oceanographers (for e.g., water mass analysis) because (i) unlike fluxes from NWP models SOSE air–sea flux estimates are dynamically consistent with ocean state variables in the sense that the latter result from a dynamical model driven by the former, and (ii) SOSE provides the entire ocean state at all points of a high-resolution grid (1/6° horizontal resolution, with 42 vertical levels).

SOSE uses different methodology than the various procedures used to construct the five other products compared here, a methodology that was introduced by the Estimating the Circulation and Climate of the Ocean (ECCO) consortium (Stammer et al. 2002). In particular, Stammer et al. (2004) estimated the time variable global air–sea heat and freshwater flux using a noneddy-resolving (1° horizontal resolution) data-assimilating ocean circulation model that adjusted the air–sea fluxes of buoyancy and momentum together with the initial temperature and salinity conditions to bring the ocean model fields into agreement with ocean observations. SOSE goes beyond this procedure in two significant ways: (i) SOSE adjusts the atmospheric state (air temperature, specific humidity, zonal and meridional wind, precipitation, and shortwave downward radiation) and derives the air–sea fluxes from the bulk formulas of Large and Pond (1981) whereas the ocean state estimate of Stammer et al. (2004) solves strictly for the surface fluxes and not the atmospheric state, and (ii) SOSE uses eddy-permitting resolution.

With respect to (i), LY09 emphasize that the physical relationships between sea surface ocean and atmospheric fields and air–sea fluxes that are embodied in the bulk formulas variables can be violated if the fluxes themselves are adjusted as in Stammer et al. (2004). This does not occur if the basic meteorological variables are adjusted and the bulk formulas are then used to compute the fluxes. With respect to (ii), resolving oceanic mesoscale features is of fundamental importance for accurate modeling of ocean circulation in general and air–sea interaction in particular. Recent satellite observations have shown intense air–sea coupling at the ocean mesoscale (Chelton et al. 2004; O'Neill et al. 2005). There is increasing evidence that mesoscale dynamical ocean processes influence the atmospheric state and should be taken into account in models such as storm prediction models (Vianna et al. 2010). Another advantage of SOSE fluxes is the optimization period, as the years 2005–07 were a time of greatly increased observational coverage due to the Argo program, which began introducing floats to the Southern Ocean in late 2003.

Since SOSE uses meteorological fields from NCEP1 as the initial guess of the atmospheric state and is also constrained within prescribed limits to the NCEP1 fields, we compare SOSE and NCEP1 air–sea fluxes to determine if SOSE modifications of NCEP1 fields reduce the known and well-documented biases of NCEP1 (Taylor 2000; Hines et al. 2000; Smith et al. 2001; Renfrew et al. 2002; Moore and Renfrew 2002; etc.). At the same time, however, as noted above, we recognize that NCEP1 has been followed by a number of improved global reanalyses. We therefore compare the SOSE fluxes with the more recent ERA (Simmons et al. 2006) and with the LY09 flux product, which is based on satellite observations and NCEP1 fields. Finally, we consider two products that represent an ad hoc approach taken by a number of investigators: apply state-of-the-art bulk algorithms

to NWP fields to obtain the turbulent (latent plus sensible) heat flux, which is subsequently combined with the unmodified net radiation from NWP fields to obtain an estimate of the air–sea buoyancy flux.

Through intercomparison of these six products, we not only attempt to assess the accuracy of SOSE fluxes, but we also attempt to gauge some of the deficiencies of various flux products and gain better insight into their relative uncertainty in different subregions. The accuracy of any flux product can only be determined by the comparison with the observations; however, such observations, particularly those sufficiently complete to characterize the climatology of 2005–07, the years studied in this paper, are presently lacking in the SO region.

We are particularly interested in the suitability of SOSE air–sea buoyancy fluxes as inputs in a calculation of Subantarctic Mode Water (SAMW) formation using the Walin (1982) formalism, which requires air–sea buoyancy fluxes at surface isopycnal outcrops as input (I. Cerovečki et al. 2011, unpublished mansuscript). The restriction to the ice-free regions follows LY09's new analysis; since SAMW forms in the ice-free regions, we can afford to focus our comparison on this region, avoiding for now the very different issues that arise in the treatment of sea ice in the various flux products. The version of SOSE that produced the flux estimates analyzed here uses a sophisticated sea ice model [the elastic–viscous–plastic solver of Hunke and Dukowicz (1997) and Hunke (2001), with imposed ice–ocean flux as in Hibler and Bryan (1987); the model is described by Campine et al. (2008) and Losch et al. (2009)]. Reproducing the ice cover is very important in determining latent and sensible heat fluxes (Simmonds and Budd 1991) as well as in determining upper-ocean stratification (Iudicone et al. 2008) and water-mass formation. SOSE reproduces the sea ice concentration quite accurately (Fig. 4 and section 4, both of Mazloff et al. 2010).

An outline of the paper is as follows. In section 2 we introduce the following six net air–sea flux estimates to be compared (they are all averaged over years 2005–07): NCEP1 and ERA, two flux products that use NCEP1 and ERA variables as input in state-of-the-art bulk flux algorithms to obtain turbulent heat flux which is combined with net radiative flux from NCEP1 and ERA to obtain the net heat flux, and finally the recently obtained SOSE and LY09 flux products. In section 3 we introduce the formulas relating buoyancy, heat, and freshwater fluxes that we use for the comparisons. The six corresponding net air–sea heat flux estimates are compared in section 4; the six corresponding freshwater and total buoyancy flux estimates are shown and discussed in section 5. Zonal averages of air–sea heat, freshwater, and buoyancy fluxes are compared in section 6. The main results are discussed and summarized in section 7. While the detailed comparison of SOSE and LY09 individual heat flux components with each other and with the NCEP1 biases from the WGASF is given in section 4, the companion comparison of NCEP1 and ERA, which provides an estimate of the uncertainties associated with air–sea heat flux products, is given in the appendix.

2. The air–sea flux products

Properties of the six datasets with which we work are given in Table 1. A list of all variables used to construct the six flux estimates analyzed in this work is given in Table 2.

a. Two NWP reanalysis air–sea flux products: ERA and NCEP1

NWP models are data-assimilating systems whose goal is operational forecasting, but they are also used to generate reanalyses in which the same ''frozen'' data assimilation system is used over the entire reanalysis time period. The quality of the air–sea flux estimates provided by reanalysis depends strongly on which numerical model and model parameterizations are used and on the quality and quantity of assimilated observations (Gulev et al. 2007). It is preferable to work with the reanalysis rather than with an operational NWP model because changes that are made to the data assimilation system in an operational NWP model (e.g., changes in GCM parameterizations) may introduce significant time discontinuities in the solution that are much greater than those typically found in the reanalysis. Siefridt et al. (1999) show that such discontinuities are particularly evident in precipitation and air–sea fluxes. A further advantage of a reanalysis is that it makes use of a significant amount of data that were not available for the initial real-time prediction (Kistler et al. 2001).

Both in reanalysis and operational forecasting, an atmospheric data assimilation system combines information coming from a weather forecast model and the available observations to diagnose the atmospheric state. NWP data assimilation is performed sequentially; as a new set of observations becomes available every 6 or 12 h, adjustments are made to the short-range forecasts to bring the model solution into consistency with observations over the assimilation window, thus providing a new analysis of the atmospheric state. The new analysis is then used as an initial state, which is propagated in time by a weather forecast model, providing a new short-range forecast. This forecast then becomes the background estimate for the new assimilation cycle. The assimilation window can be of short temporal duration, which is technically convenient, or cover longer periods, in which

TABLE 1. The main characteristics of the six air–sea heat flux datasets considered in this work.

Group	Air–sea flux dataset	Sampling of data	Horizontal resolution
NWP analyses	NCEP1 (Kalnay et al. 1996)	4 times daily	192 × 94 points in lat/lon (approx. 2°), global Gaussian grid with variable resolution
	ERA	4 times daily	0.703° × 0.702° (global Gaussian grid with 512 × 256 points in lat/lon)
NWP radiation and COARE 3.0 turbulent flux algorithm (Fairall et al. 2003) using NWP inputs	NCEP1+COARE 3.0	4 times daily	192 × 94 points in lat/lon (approx. 2°), global Gaussian grid with variable resolution
	ERA+COARE 3.0	4 times daily	0.703° × 0.702° (global Gaussian grid with 512 × 256 points in lat/lon)
Hybrid analyses	SOSE (Mazloff et al. 2010)	5-day averages	1/6° × 1/6°
	LY09	Daily averages	1° × 1°

case the reproduced state will have fewer discontinuities in time and therefore be more physically realistic. In all cases, however, the sequential adjustments introduce jumps in the model fields, so the resulting atmospheric analysis does not evolve in complete accordance with model equations. (SOSE, described below in section 3, is nonsequential in that there is only one assimilation window covering the entire period of simulation and thus avoiding dynamical discontinuities.)

We analyze air–sea flux products from the ERA and NCEP1; as noted above, the latter is needed to estimate and discuss SOSE adjustments to the NCEP1 derived initial guess fields. Neither NCEP1 nor ERA has an ocean model as part of their system. Instead, they prescribe the sea surface temperature as a boundary condition. NCEP1 uses the Reynolds reanalysis sea surface temperature (Reynolds and Smith 1994, 1995) and ERA uses National Oceanic and Atmospheric Administration

TABLE 2. The list of input variables considered in this work.

Group	Air–sea flux dataset and its source	Sampling of data	Atmospheric state variables used in this work
NWP analyses	NCEP1, NOAA/Oceanic and Atmospheric Research (OAR)/Earth Systems Research Laboratory (ESRL) Physical Sciences Division (PSD), Boulder, Colorado (available at http://www.cdc.noaa.gov/)	6-h average	Sensible heat flux, latent heat flux, downward shortwave and longwave radiation, net shortwave and longwave radiation, precipitation, evaporation
		Instantaneous values every 6 h	Air temperature, air pressure, relative humidity, zonal and meridional components of wind velocity, sea surface temperature
	ERA from the Research Data Archive (RDA) at the National Center for Atmospheric Research (NCAR), dataset number ds627.0	6-h forecast at 0000 and 1200 UTC and 12-h forecast at 0000 and 1200 UTC	
		Instantaneous values	Air temperature, air pressure, dewpoint temperature, zonal and meridional component of wind velocity, sea surface temperature
		6- and 12-h averages	Surface sensible heat flux, surface latent heat flux, evaporation, surface solar radiation downward, surface thermal radiation downward, net surface solar radiation, net surface thermal radiation
Hybrid analyses	SOSE (available at http://sose.ucsd.edu/DATA/SOSE/sose_stateestimation_data.html)	5-day averages	Sensible heat flux, latent heat flux, net shortwave and longwave radiation, freshwater flux, sea surface temperature, sea surface salinity
	LY09 from the Research Data Archive (RDA) at NCAR, dataset number ds260.2	Daily averages	Evaporation, precipitation, runoff, latent heat flux, sensible heat flux, downward and upward longwave radiation, net shortwave radiation

(NOAA) real-time global (RTG) sea surface temperature analyses (Thiebaux et al. 2003).

b. Two air–sea flux products incorporating the COARE 3.0 algorithm

These were constructed using ERA and NCEP1 meteorological and oceanic surface variables as input into the state-of-the-art Coupled Ocean–Atmosphere Response Experiment (COARE) 3.0 algorithm (Fairall et al. 2003) to estimate the sensible and latent heat fluxes. They were then combined with the corresponding unmodified net radiation products provided by the ERA and NCEP1 to obtain the net air–sea heat flux estimates, to which we hereafter refer as "ERA+C" and "NCEP1+C". We make use of the COARE 3.0 bulk flux algorithm because it produces the smallest biases in estimated latent and sensible heat fluxes when compared to direct turbulent flux measurements (Brunke et al. 2002, 2003). Although the COARE 3.0 bulk flux algorithm has been modified to remain valid for higher wind speeds and valid globally rather than being hardwired to the tropical values for which it was originally developed, one needs to keep in mind that the COARE 3.0 bulk flux algorithm was not originally developed for high latitudes and it has not been tested for wind speeds higher than 10 m s^{-1} (Fairall et al. 2003). Therefore, the COARE 3.0 bulk flux algorithm might still have large uncertainties in regions of high wind speeds, such as the Southern Ocean. Additional motivation for constructing ERA+C and NCEP1+C flux estimates was provided by the results of Renfrew et al. (2002) and Moore and Renfrew (2002), who, analyzing the Labrador Sea and western boundary current regions, recommended using NCEP surface meteorological fields as input into a more appropriate bulk algorithm rather than using the turbulent heat flux estimates from the NCEP NWP model. We shall see, however, that introduction of the more accurate bulk flux algorithm to improve two of the four components of the net air–sea flux may result in an apparently less accurate net heat flux product, at least for the Southern Ocean.

c. Two recent air–sea flux products: LY09 and SOSE

These were developed as an improvement to NCEP flux estimates, each using a very different methodology. LY09 is a global estimate of air–sea heat and freshwater flux. The input data for the near surface vector wind, atmospheric temperature, specific humidity, and air density are based on NCEP1. The input data for radiation, sea surface temperature, sea ice concentration, and precipitation come from a variety of satellite-based products. The approach of LY09 was to use accurate historical observations to either reduce the known global biases of input variables provided by NCEP1 or to adjust surface radiation estimates of the International Satellite Cloud Climatology Project flux data (Zhang et al. 2004). LY09 ensured a balanced global freshwater and heat flux budget, in which the globally integrated net fluxes are close to zero. Unlike SOSE, the radiation and precipitation from NCEP1 were not utilized by LY09 in any way.

SOSE, like the NWP systems, is a data assimilation system, but SOSE is an ocean assimilation, whereas NWP products are atmospheric assimilations. The goal of NWP is prediction, and thus the machinery used is aimed toward this goal at the expense of exact physics. In SOSE, the physics of the ocean model is a hard constraint not to be violated. The SOSE solution is accomplished by iteratively and systematically solving for input parameters that include the initial conditions (temperature, salinity) and the atmospheric state. The result of each iteration is an updated set of input parameters used to run the model forward in time for the entire time period of 3 yr. The SOSE solution thus is continuous in time and strictly obeys the model dynamics. Mazloff et al. (2010) evaluated SOSE performance by comparing the solution with in situ ocean temperature and salinity observations, altimetry, and sea ice data, and showed it to be, for the most part, consistent with ocean observations. Here, we focus on the SOSE determined air–sea heat and freshwater fluxes.

3. Relationship between buoyancy, heat and freshwater fluxes

The buoyancy flux B is composed of heat and freshwater contributions B_{HF} and B_{FW}, for example, Gill (1982):

$$B = B_{\mathrm{HF}} + B_{\mathrm{FW}} = (g/\rho_0)[(\alpha Q_{\mathrm{HF}})/c_p - \rho_0 \beta S(E - P)], \quad (1)$$

where g is the gravitational acceleration, ρ_0 is a reference density, c_p is the specific heat for seawater, S is ocean surface salinity, α and β are the thermal expansion and saline contraction coefficients (both functions of temperature, salinity, and pressure), and Q_{HF} is the net air–sea heat flux (positive for ocean heat loss; W m^{-2}). Also, E is evaporation, and P is precipitation (E and P both positive; m s^{-1}). Runoff is included in the fields at the boundary points of the ocean. Positive buoyancy flux implies a decrease in ocean surface buoyancy (increase in surface density associated with a decrease in either sea surface temperature or an increase in evaporation minus precipitation).

To readily compare the relative importance of the heat and freshwater contributions, we follow the approach of, for example, Moore and Renfrew (2002), and express the buoyancy and freshwater fluxes as heat-equivalent

fluxes (W m^{-2}), denoted Q_{BF} and $Q_{FW,}$ respectively. The heat-equivalent buoyancy flux is a sum of air–sea heat flux and freshwater heat-equivalent flux

$$Q_{BF} = Q_{HF} + Q_{FW} = \frac{\rho_0 c_p}{g\alpha} B, \tag{2}$$

and the freshwater heat-equivalent flux Q_{FW} is given by

$$Q_{FW} = \frac{\rho_0 c_p}{g\alpha} B_{FW} = -\frac{\rho_0 c_p}{\alpha} \beta S(E - P). \tag{3}$$

For a typical β/α a heat flux of 1 W m^{-2} contributes approximately the same ocean buoyancy flux as a freshwater flux of 1 mg m^{-2} s^{-1}, or in terms of evaporation and precipitation, approximately 0.0864 mm day^{-1} or approximately 3.1 cm yr^{-1} at 5°C (Large and Nurser 2001).

We consistently call the term Q_{HF} the *net air–sea heat flux* (the sum of upward and downward shortwave radiative heat flux, upward and downward longwave radiative heat flux, sensible and latent heat flux components) and the terms Q_{FW} and Q_{BF} the *freshwater heat-equivalent flux*, and the *buoyancy heat-equivalent flux*, respectively. This convention enables one to readily compare the heat flux and freshwater flux contributions to the buoyancy flux, which is particularly important in high southern latitudes, where buoyancy flux depends strongly on net freshwater input as well as on net heat flux.

Since the magnitude of the thermal expansion coefficient α decreases strongly as water temperature decreases, while the haline contraction coefficient β remains relatively unchanged (Moore and Renfrew 2002), the ratio β/α increases with decreasing sea surface temperature, making the freshwater flux contribution to the surface buoyancy flux increasingly important relative to that of the heat flux in regions with colder sea surface temperatures. In the polar regions of the Southern Ocean the freshwater flux contribution to the buoyancy flux is of larger magnitude than the net heat flux contribution to the buoyancy flux (see section 5). Thus, in many regions with ocean heat loss, excess precipitation and melting give rise to a net oceanic buoyancy gain instead of a buoyancy loss. This somewhat counterintuitive result has been previously noted (e.g., Warren et al. 1996; Speer et al. 2000; Karsten and Marshall 2002).

4. The net air–sea heat flux

a. NWP models: NCEP1 and ERA

The net air–sea heat fluxes, averaged over years 2005–07, estimated by NCEP1 and ERA are quite similar (Figs. 1a,b). As expected, the most intense ocean heat loss is over the western boundary currents (the Agulhas Current and Agulhas Retroflection region, the East Australian Current, and the Brazil Current), while weaker ocean heat loss is in the subtropical gyres and in a band just equatorward of the Sub-Antarctic Front (SAF) in the Pacific Ocean. The ocean gains heat over the northward flowing Malvinas Current and along the eastern boundaries of the South Atlantic (Benguela Current system) and South Pacific (Peru–Chile Current system), where upwelling of cold water occurs. The northern Weddell Sea, where cold polar waters are brought into contact with the more temperate atmosphere, is a region of strong ocean heat gain.

The NCEP1 net ocean heat loss tends to be more intense than the corresponding ERA net ocean heat loss (Fig. 2b). Noteworthy are the small-scale regions of ERA intense ocean heat loss extending south and southeast from the southern tip of Africa along the northern edge of the SAF to Drake Passage. These small-scale features are nearly completely absent in the generally smoother NCEP1 mean net heat flux.

b. COARE3.0 turbulent heat fluxes with NWP inputs

We next consider the net air–sea heat fluxes computed as in section 4a, but replacing the sensible and latent heat fluxes with those calculated using the COARE 3.0 bulk algorithms with basic input fields from NCEP1 and ERA (NCEP1+C and ERA+C). Both "with-COARE" estimates yield excessive unrealistic net ocean heat gain over much of the Southern Ocean (Figs. 1e,f). In the subtropics, the net ocean heat loss is unrealistically small so that the zonally integrated heat flux is positive (ocean heat gain) at all latitudes (discussed further in section 6). Overall, the with-COARE net air–sea heat flux is biased toward producing a warmer ocean, as seen when comparing "ERA+C" with ERA (Fig. 2a) and "NCEP1+C" with NCEP1 (Fig. 2i) net air–sea heat flux estimates. The difference between the net air–sea heat flux estimates from reanalysis and with-COARE estimates is largest in the regions of most intense ocean heat loss, such as the western boundary currents (Figs. 2a,i).

A possible reason for this bias may be that with-COARE latent and sensible ocean heat losses are too weak. However, it is also possible, and even likely, that the sensible and latent heat flux estimates obtained using reanalysis input fields in COARE 3.0 are more accurate than the reanalysis fluxes themselves (as in Brunke et al. 2003; and similar to results quoted in Renfrew et al. 2002; Moore and Renfrew 2002), but combining the with-COARE turbulent fluxes with the unchanged radiative reanalysis fluxes may lead to degraded net air–sea heat fluxes. Previous works showing the cancellation of biases of individual air–sea heat flux components of

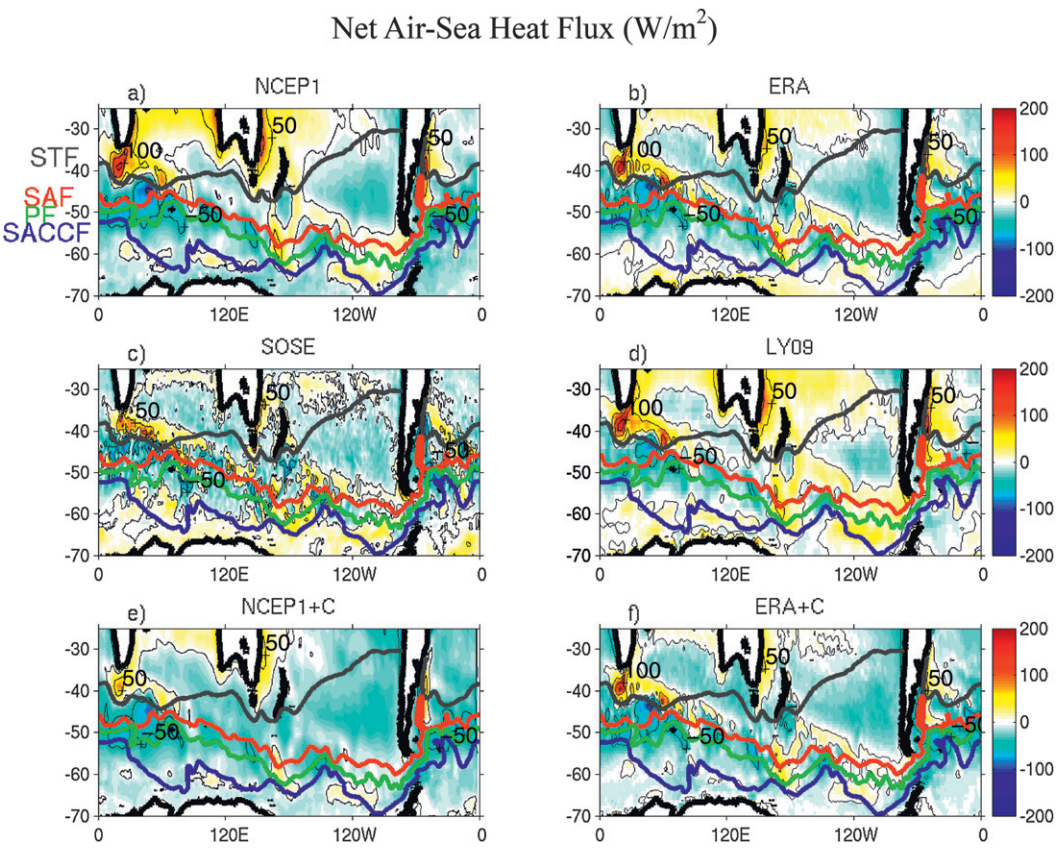

FIG. 1. The time average over years 2005–07 of the net air–sea heat flux (the sum of latent, sensible, net longwave, and net shortwave heat flux components; W m^{-2}), estimated by (a) NCEP1, (b) ERA, (c) SOSE, (d) LY09; the time average for years 2005–07 of net air–sea heat flux obtained by combining sensible and latent heat flux estimates from COARE 3.0 algorithm using all input variables describing the atmospheric state from (e) NCEP1 with the NCEP1 net longwave and net shortwave radiative fluxes, and (f) as in (e), but for ERA. The sign convention for this and all subsequent figures is that positive values correspond to upward heat flux out of the ocean (ocean heat loss); thus in general positive fluxes correspond to ocean surface density increase whether by heat loss or by net freshwater loss. Contour interval is 50 W m^{-2}. Thick colored lines are climatological positions of the fronts given by Orsi et al. (1995): subtropical front (ST, black), subantarctic front (SAF, red), polar front (PF, green), and southern ACC front (SACC, blue).

a particular net air–sea heat flux product support the latter possibility. For instance, the WGASF shows that in the Drake Passage latitude band the NCEP1 net shortwave (NSW) radiation is biased high (yielding too strong ocean heat gain) but this is partially compensated by the latent heat flux bias (yielding too much ocean heat loss). Weller et al. (2004) show similar examples of cancellation of biases of NCEP1 NSW and latent heat flux. Therefore if one were to correct only the turbulent heat flux component from reanalysis in regions where the sensible and latent heat loss is too strong, leaving the radiative components unchanged, the resulting net air–sea heat flux would show insufficient ocean heat loss. This may explain the warm bias in the with-COARE net heat flux estimates.

Both the NCEP1 NSW radiation bias and NCEP1 sensible and latent heat flux bias have been well documented. Overall, it has been shown that NCEP1 NSW radiation is biased high, overestimating ocean heat gain (e.g., Röske 2006; da Silva and White 1996), especially in regions where low-level stratiform clouds are the dominant cloud type—for example, the Australian subtropical region, the Peruvian region, and the Southern Ocean (Klein and Hartmann 1993; Scott and Alexander 1999). Other studies have shown that NCEP overestimates sensible and latent heat flux compared to the observed fluxes in moderate to high wind speed regimes; this problem is most acute when air–sea temperature differences, and consequently the sensible heat flux, are large (Renfrew et al. 2002; Moore and Renfrew 2002). It has also been shown that overestimating shortwave radiation at the surface is a more general problem, present not only in NCEP1 but also in a number of the GCMs

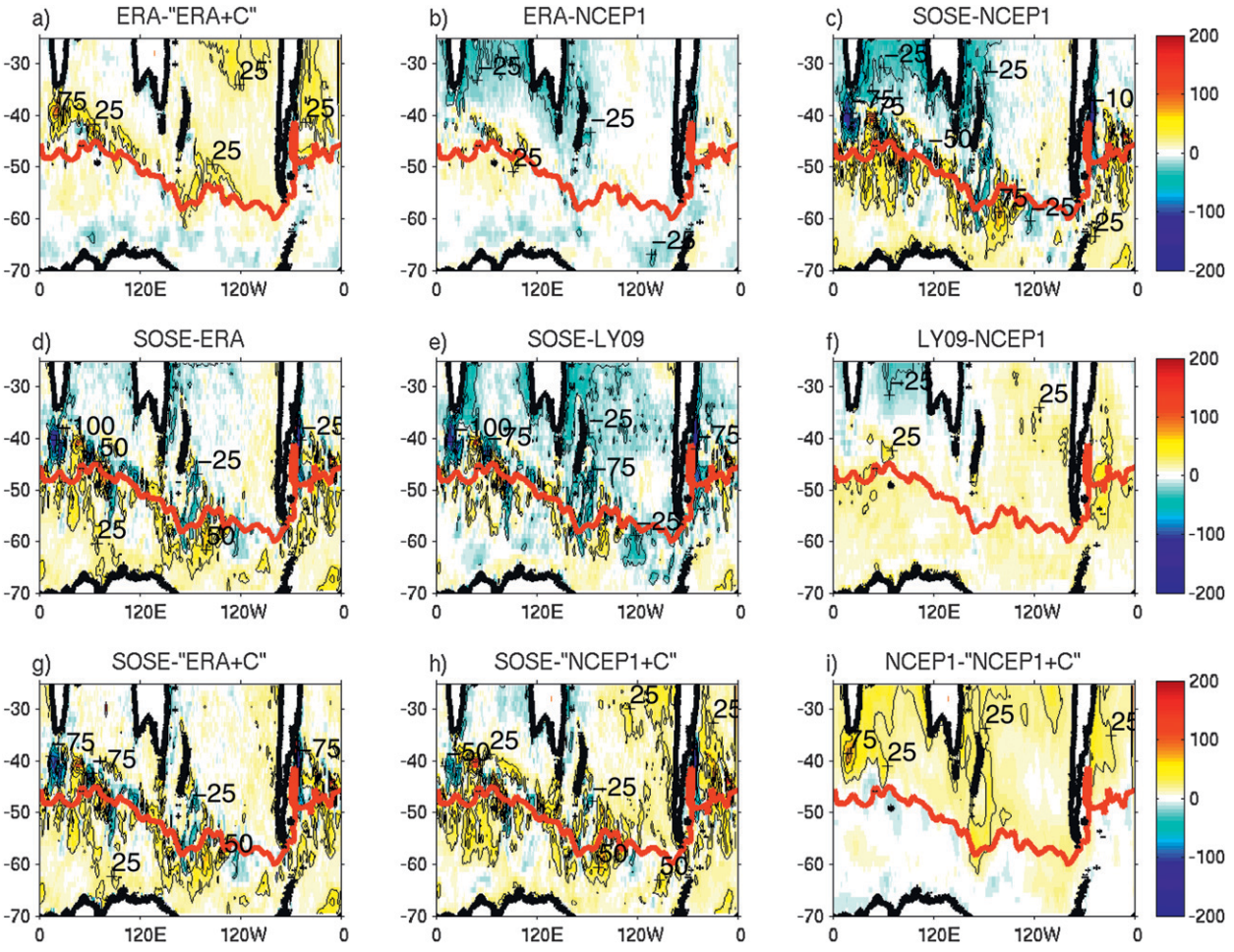

FIG. 2. Difference between time-averaged (years 2005–2007) net heat flux estimates, all interpolated on 1° × 1° grid, contour interval 25 W m^{-2}. Titles identify source of flux estimates. The red curve is the subantarctic front, as in Fig. 1.

(e.g., Wild 2005) because they tend to underestimate atmospheric solar absorption, predominantly by water vapor, aerosol, and clouds. The exclusion of strongly absorbing aerosols in GCMs can regionally cause excessive insolation at the ground (e.g., Cusack et al. 1998). The crude aerosol climatologies typically used in current GCMs and reanalyses do not properly account for these aerosol effects (Wild 1999), thus introducing a bias not only in NSW radiation estimates, but also in, for example, the oceanic heat distribution (Cai et al. 2006).

c. *SOSE and LY09*

We next turn to the SOSE and LY09 air–sea heat flux products, which are quite different from the reanalyses. The differences between SOSE and NCEP1 net air–sea heat flux estimates are overall similar to the differences reported in the state estimate of Stammer et al. (2004), which was developed using the same method as the SOSE (cf. our Fig. 2c with Stammer et al.'s Fig. 3). To determine whether the SOSE adjustments of the NCEP1 atmospheric state, made as a part of the SOSE optimization procedure, represent a true improvement of the NCEP1 fields, we follow the procedure of Stammer et al. (2004), who concluded the air–sea fluxes from their state estimate were an improvement to the NCEP1 by comparing with the Large and Yeager (2004) flux estimates. Here, we compare the SOSE air–sea flux estimates (Fig. 1c) with the most recent version of the LY09 air–sea flux estimate, LY09 (Fig. 1d).

Considering that SOSE and LY09 air–sea heat fluxes are obtained using different methods and observations to construct the fluxes (LY09 is based on atmospheric observations and SOSE is constrained by oceanic observations), they show remarkable similarity in the large-scale pattern of their differences from NCEP1 (Figs. 3a,b). This does not necessarily imply that LY09 and SOSE flux products are more accurate than NCEP1, but it gives confidence in the data and procedures used

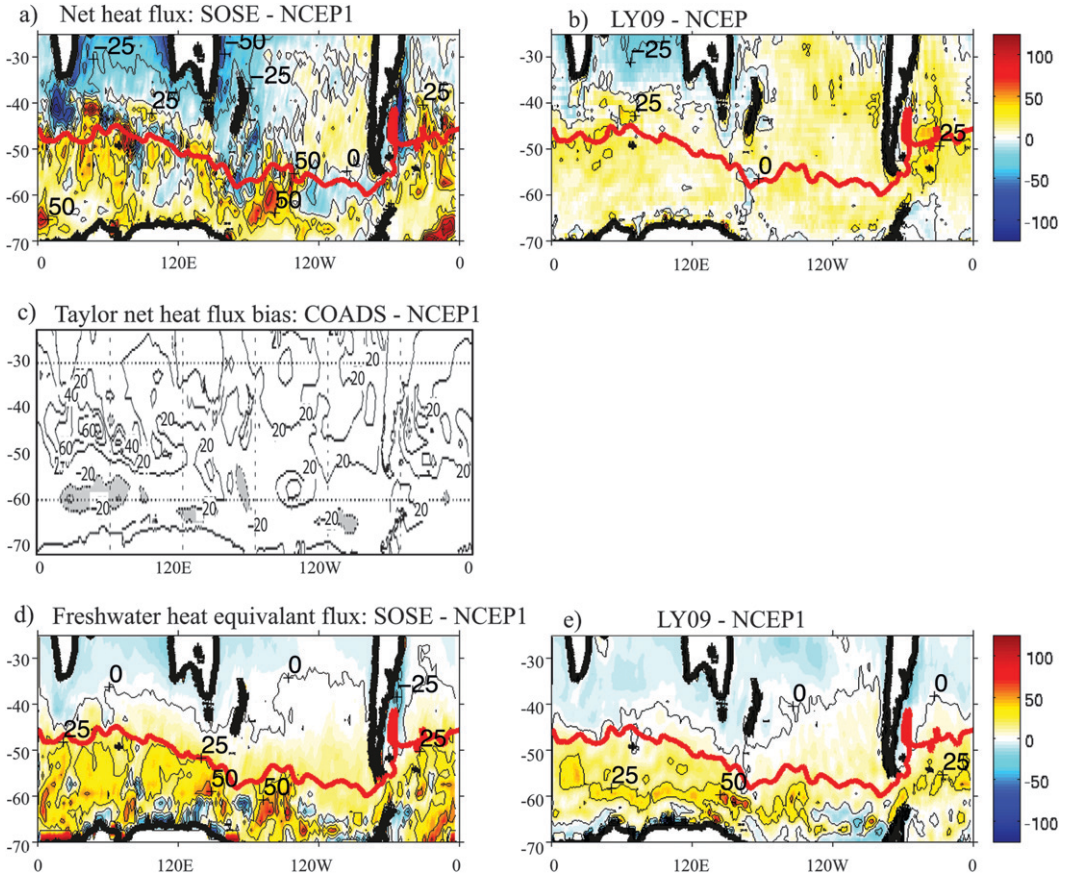

FIG. 3. The time average over years 2005–07 of (a) the difference between SOSE and NCEP1 net air–sea heat flux (W m^{-2}) where each is the sum of latent, sensible, net longwave, and net shortwave heat flux component, (b) as in (a) but for LY09, and (c) NCEP1 net heat flux bias, modified from Fig. 11.4.23(e) of Taylor (2000), where the reference dataset is the original UWM/COADS dataset by da Silva et al. (1994) averaged over years 1981–92. Bias is shown as COADS minus NCEP1 net heat flux estimate, where positive bias indicates that NCEP1 net ocean heat loss (gain) is stronger (weaker) than in COADS. Contour interval is 20 W m^{-2}; regions with negative values are shaded. (d) The difference between SOSE and NCEP1 freshwater heat-equivalent flux from Eq. (3); (e) as in (d), but for LY09. Contour interval is 25 W m^{-2}. All fields in (a),(b),(d),(e) are interpolated on 2° × 2° grid. The red curve is the subantarctic front, as in Fig. 1.

for developing each. To fully assess the accuracy of the SOSE and LY09 flux products would require a comparison with observations at the level of detail of WGASF, a comparison beyond the scope of this paper.

Both SOSE and LY09 increase net ocean heat loss relative to NCEP1 in the polar regions (adjacent and poleward of SAF), in the southeastern Pacific and southwestern Atlantic, and they both decrease the net ocean heat loss in subtropical Indian Ocean and eastern Atlantic and over the western boundary currents (Figs. 3a,b). SOSE differences from NCEP1 fields are larger than the corresponding LY09 differences. Compared with LY09, SOSE net air–sea heat flux shows overall more ocean heat gain/less ocean heat loss almost everywhere in the domain, most notably over the regions with the largest ocean heat loss such as the western boundary currents. We also note that SOSE introduces small-scale regions of ocean heat loss extending south and southeast of the southern tip of Africa, which are present in the ERA but not the coarser-resolution NCEP1 net heat flux estimates.

The WGASF estimated the NCEP1 biases relative to the reference datasets they considered to be most accurate. The reference dataset for NSW and NLW was the surface radiation budget (SRB) of Darnell et al. (1992), which is based on satellite measurements. The WGASF emphasized that, although satellite estimates of surface NSW are more reliable than the other global estimates of surface NSW, they can differ substantially from point surface measurements, as shown by White (1996). The reference dataset for the latent and sensible heat flux was the original University of Wisconsin—Milwaukee (UWM)/Comprehensive Ocean–Atmosphere Dataset (COADS) data of da Silva et al. (1994). The reference

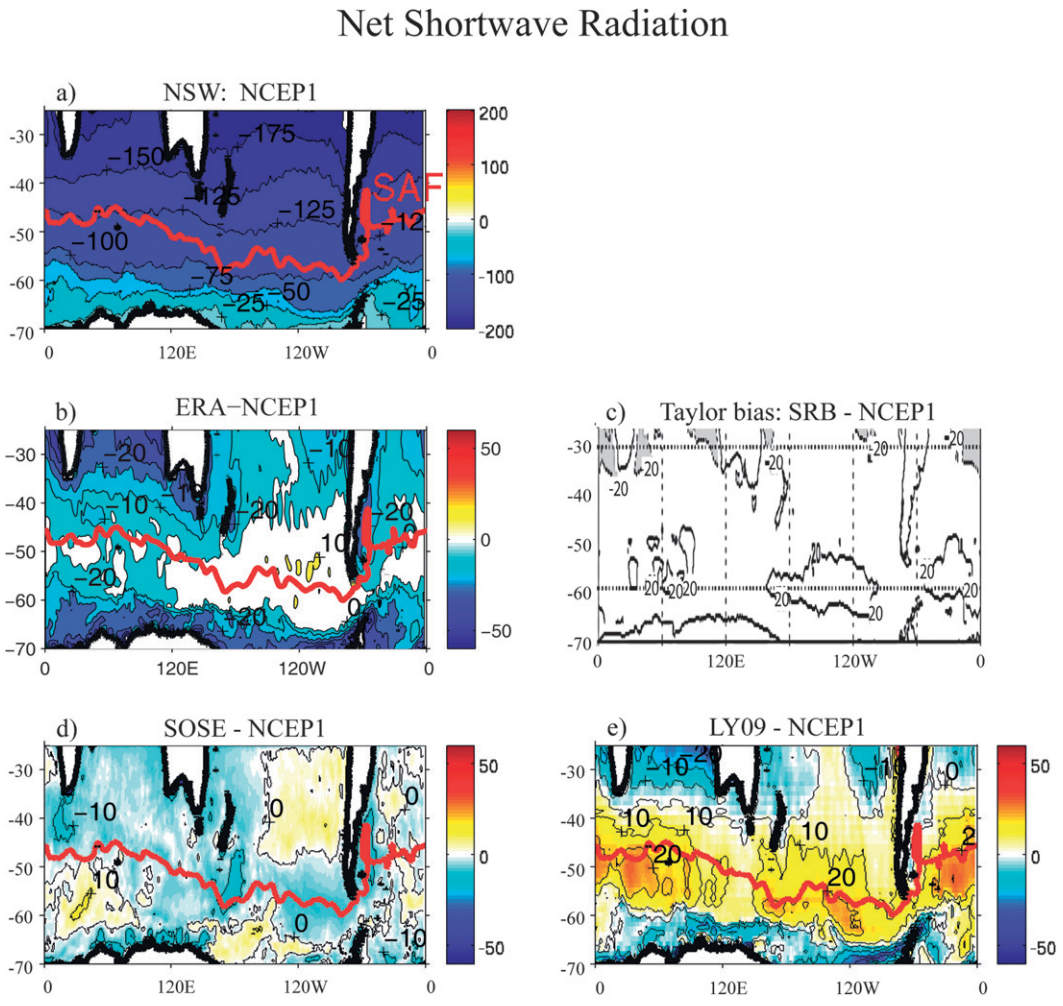

FIG. 4. The time average for years 2005–07 of NSW (W m^{-2}) (a) from NCEP1, (b) difference of ERA minus NCEP1, (c) NCEP1 NSW bias from Taylor (2000), modified from their Fig. 11.4.13(e), where the reference dataset is SRB of Darnell et al. (1992) averaged from July 1983–June 1991. Bias is shown as SRB minus NCEP1 NSW radiation, where positive bias indicates that NCEP1 NSW radiation is stronger (leading to more surface ocean heat gain) than in SRB. (d) SOSE minus NCEP1 NSW radiation, and (e) as in (d), but for LY09. Contour interval in (a) is 25 W m^{-2}, (c) 20 is W m^{-2} with zero contour omitted and positive values shaded, and (b),(d),(e) are 10 W m^{-2}. The red curve is the subantarctic front, as in Fig. 1.

dataset for the net heat flux was the tuned UWM/COADS estimate of da Silva et al. (1994). All the reference datasets used in the WGASF are time averaged over approximately a decade.

We next consider the SOSE and LY09 adjustments of the four individual heat flux components separately to determine if and which of them tend to reduce the NCEP1 heat flux bias determined by the WGASF. The analogous comparison of the four individual heat flux components of NCEP1 and ERA provides an estimate of the uncertainties associated with net air–sea heat flux estimates in general but is less central for this work and is thus given in the appendix.

1) SOSE AND LY09 NSW AND NLW RADIATION

The WGASF shows that NCEP1 NSW radiation is too weak (thus insufficient ocean heat gain, negative bias) in the subtropics and too strong in the Drake Passage latitude band (~40°–60°S) in comparison with the reference SRB dataset (Fig. 4c). Scott and Alexander (1999) attribute both biases to NCEP1 treatment of clouds—the negative NCEP1 NSW radiation bias in the subtropics is attributed to model errors in treating the cumulus clouds, and positive NCEP1 NSW radiation bias in the high latitudes is attributed to inadequate representation of the dominant low-level stratiform clouds where NCEP1 has

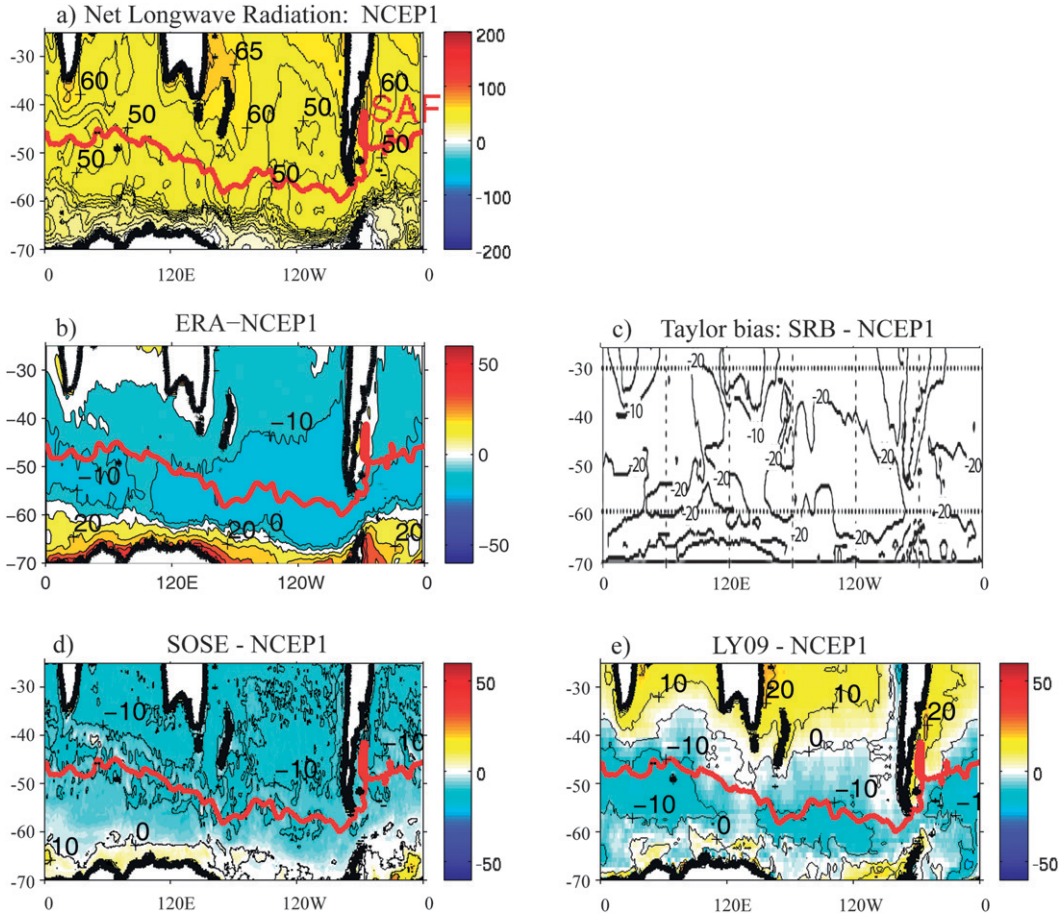

FIG. 5. As in Fig. 4, but for NLW. (c) NCEP1 NLW bias from Taylor (2000), Fig. 11.4.19(e). Contour interval is 10 W m^{-2} in (d) with zero contour omitted and positive values shaded. The positive bias indicates that NCEP1 NLW radiation is stronger (leading to more surface ocean heat loss) than in SRB. The red curve is the subantarctic front, as in Fig. 1.

less total cloud fraction than in observations (Scott and Alexander 1999).

The WGASF finds that in the regions with bias, the NCEP1 ocean heat loss by net longwave (NLW) radiation is always larger than in the SRB reference dataset (Fig. 5c). The WGASF attributes the NCEP1 NLW biases in the eastern subtropical oceans to problems in the NCEP treatment of low-level stratus clouds. Large biases of up to 20 W m^{-2} were also found in the latitude band of roughly 40°–60°S, and similarly (up to 20 W m^{-2}) around the Antarctic continent. In some regions along 60°S this bias is cancelled by NCEP1 NSW radiation bias. LY09 tend to reduce both the NCEP1 NSW and NLW bias (cf. Figs. 4c,e and 5c,e); they increased ocean heat gain (loss) by NSW (NLW) radiation in the subtropics and they decreased ocean heat gain (loss) by NSW (NLW) radiation in the latitude band of roughly 40°–60°S. SOSE has a tendency to reduce NSW biases, although not in all regions and not to the same degree (Figs. 4d and 5d). SOSE decreased NCEP1 NLW not only in the regions with bias as estimated by WGASF but everywhere, except in the narrow band around Antarctica (Fig. 5d).

2) SOSE AND LY09 LATENT AND SENSIBLE HEAT FLUXES

In some subtropical regions and in the Drake Passage latitude band (~40°–60°S), NCEP1 latent ocean heat loss is predominantly biased high; WGASF attributes this bias to NCEP1 bulk flux formulas, which overestimate latent heat loss under conditions of high wind, especially when combined with large air–sea temperature difference (also Smith et al. 2001; Moore and Renfrew 2002). Both the large-scale pattern and the magnitude of the LY09 and SOSE latent heat flux adjustments to NCEP1 are similar to each other (Figs. 6e,f). They both tend to decrease NCEP1 latent heat loss in the subtropics and the western boundary currents reducing the NCEP1 bias. Along and

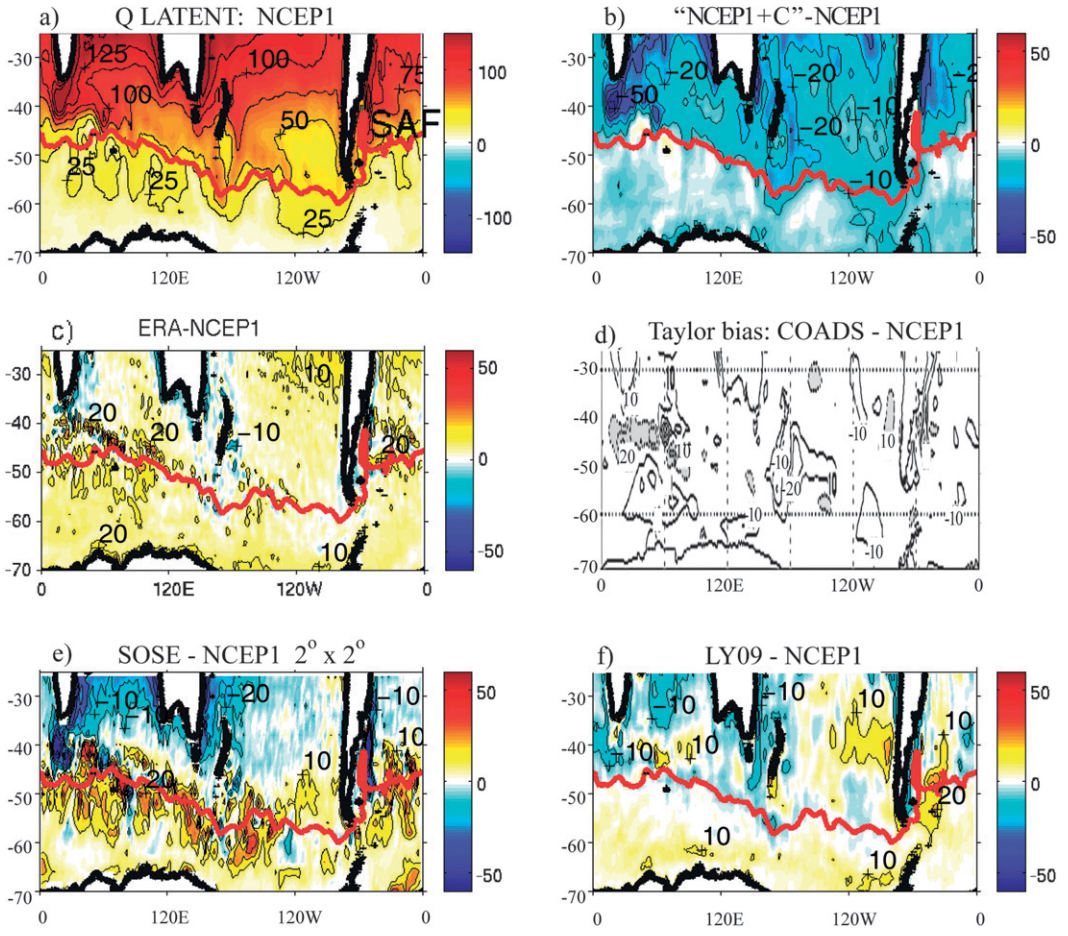

FIG. 6. The time average over years 2005–07 of latent heat flux: (a) estimate by NCEP1; (b) NCEP1+C minus NCEP1; (c) ERA minus NCEP1; (d) NCEP1 latent heat flux bias modified from Fig. 11.4.2d of Taylor (2000) (only the latitude band 25°–90°S is shown), where the reference dataset is the original UWM/COADS data by da Silva et al. (1994) averaged over years 1981–92; NCEP1 bias is shown as UWM/COADS data minus NCEP1, so that positive bias indicates that NCEP1 latent heat loss is stronger than in COADS, (e) SOSE minus NCEP1, (f) LY09 minus NCEP1. Contour interval in (a) is 25 W m^{-2} and (b)–(f) is 10 W m^{-2} with zero contour omitted; in (d) positive values are shaded. In (e) fields are interpolated on 2° × 2° grid. Positive values indicate latent heat loss from the ocean. The red curve is the subantarctic front, as in Fig. 1.

poleward of the SAF, both SOSE and LY09 increase the latent heat loss by increasing the wind speed and decreasing the specific humidity (not shown). Overall, the LY09 differences from NCEP1 are smaller in magnitude than the SOSE differences. As noted in section 4b, the WGASF estimates of NCEP1 NSW and latent heat flux bias show that in many regions these two biases are of opposite sign (e.g., west of Australia, subtropical South Atlantic, central subtropical South Pacific) so that they tend to cancel in the NCEP1 net heat flux product.

The sensible heat loss is much smaller in magnitude than the latent heat loss. While most of the ocean experiences sensible heat loss, there is a broad band of sensible heat gain (NCEP1) or near neutrality (e.g., SOSE) along the Antarctic Circumpolar Current (ACC; roughly the SAF in the figures), which is a broad upwelling region. Both SOSE and LY09 increased the NCEP1 sensible heat loss (to greater loss) almost everywhere (Figs. 7e,f) except for LY09 adjustments in some subtropical regions. In NCEP1+C, ERA and LY09 flux products (Figs. 7b,c,f) sensible heat loss is weaker in the subtropics and stronger everywhere else relative to NCEP1, which tends to correct the NCEP1 sensible heat flux bias as estimated by WGASF. WGASF estimates the largest NCEP1 sensible heat flux bias (too much ocean heat loss) to be along 60°S, which is the latitude band where sensible heat flux exhibits large variability (Fig. 7d). WGASF show that around Antarctica NCEP1 sensible heat loss should be increased. Both SOSE and LY09 make this adjustment. The general increase in wind speed in both

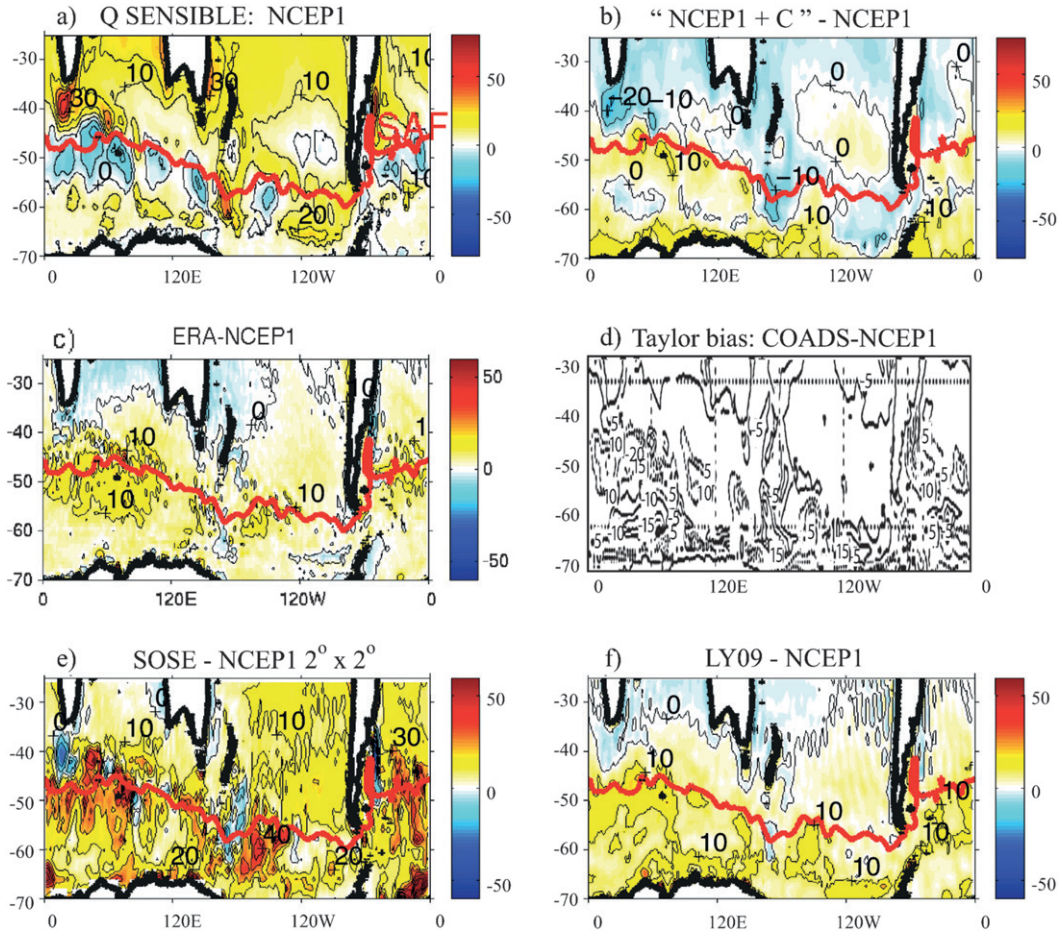

FIG. 7. As in Fig. 6, but for sensible heat flux component (W m^{-2}). (d) NCEP1 sensible heat flux bias modified from Fig. 11.4.10 (d) of Taylor (2000), where positive bias indicates that NCEP1 sensible heat loss is stronger than in COADS is shown. Contour interval is 10 W m^{-2}, in (d) with zero contour omitted and positive values shaded. The red curve is the subantarctic front, as in Fig. 1.

LY09 and SOSE contributed to an increase of sensible oceanic heat loss, most notably south of SAF.

A major NCEP1 net air–sea heat flux bias according to the WGASF is an overly strong ocean heat loss in the subtropics and in the western boundary current regions (both compared with the COADS estimate), in particular in the Agulhas Current and Agulhas Return Current region (Fig. 3c). Both SOSE and LY09 correct this bias in both places by correcting the bias of the individual heat flux components. In the subtropics, SOSE and LY09 decreased latent ocean heat loss and increased NSW> radiation, but in SOSE ocean heat loss by both NLW and latent heat flux is smaller than in LY09 in the subtropical region. This contributes to the overall main difference between the SOSE and LY09 net air–sea heat flux estimates, which is that SOSE estimates considerably less ocean heat loss (more ocean heat gain) than LY09, especially in the subtropics. This weak net ocean heat loss in SOSE may be partly attributed to the open boundary condition; the coarse resolution (1°) ocean state estimate by Forget (2010), which SOSE uses as the open boundary condition shows similarly weak ocean heat loss (not shown).

Both SOSE and LY09 corrected the NCEP1 net air–sea heat flux bias over the subtropical western boundary currents (East Australian Current, Agulhas Current and Agulhas Return Current, and Brazil Current), reported by the Taylor (2000), Smith et al. (2001), Renfrew et al. (2002), Moore and Renfrew (2002), and Yu and Weller (2007), by decreasing net ocean heat loss, predominantly by decreasing latent heat flux. In both SOSE and LY09, increased ocean heat loss in the polar regions is a result of an increase of both latent and sensible heat flux, and this is partly due to increased wind speed relative to NCEP1.

d. Correlations between 5-day-averaged heat flux estimates

To compare the short-term variations in various heat flux products, we computed the correlations between

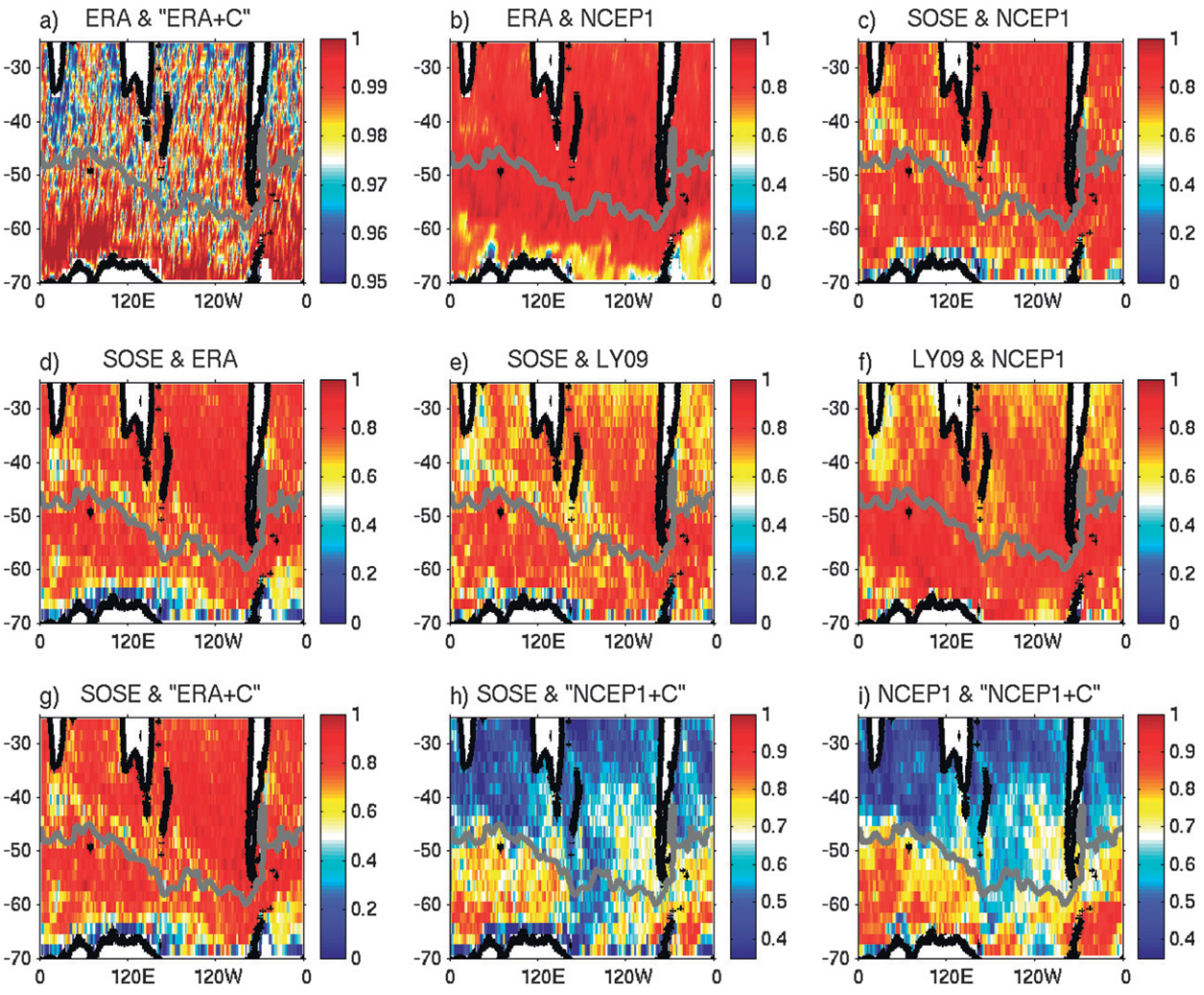

FIG. 8. Three-year average of correlations between 5-day mean heat flux anomalies shown in Fig. 2. Note different color scales for (a), (b)–(g),(h), and (i). The gray line is the subantarctic front.

pairs of 5-day-averaged anomalies (hereafter 5-day correlations). The anomalies are defined as differences of 5-day-averaged net air–sea heat flux estimates away from the sum of the mean (which is calculated over 3 yr) and the seasonal cycle (which is represented by a fit of sine and cosine functions with periods of a half year and a year to the original heat flux field).

The highest 5-day correlation between any two net heat flux products considered here is between ERA and ERA+C (Fig. 8a), where the correlations are uniformly

TABLE 3. The correlation coefficients between 5-day-averaged anomalies (defined in section 4d) for years 2005–07 of net air–sea net heat flux and $E - P$ (boldface), shown in Figs. 12 and 14, over the ocean south of 24.7°S. For the comparison, all datasets are interpolated on a 1° × 1° grid. ''No FW'' means that there is no independent freshwater flux estimate.

	NCEP1	ERA	NCEP1+C	ERA+C	SOSE	LY09	
NCEP1	—	0.69	0.15	0.68	0.59	0.35	Net heat flux correlations
ERA	**0.61**	—	0.12	0.95	0.53	0.27	
NCEP1+C	**No FW**	**No FW**	—	0.12	0.11	0.11	
ERA+C	**No FW**	**No FW**	**No FW**	—	0.53	0.34	
SOSE	**0.62**	**0.14**	**No FW**	**No FW**	—	0.27	
LY09	**0.14**	**0.14**	**No FW**	**No FW**	**0.11**	—	
			Net $E - P$ correlations				

very high (Table 3). SOSE correlations with NCEP1, ERA, and ERA+C (Figs. 8c,d,g) are similar both in magnitude and the large-scale pattern, showing lower correlations (~0.4) in regions of high mesoscale activity such as the ACC, Agulhas Current, and Agulhas Retroflection region, and Brazil–Malvinas Current confluence region and higher correlations (~0.8) in the other regions. Although the large-scale pattern of net air–sea heat flux estimated by SOSE and LY09 is quite similar, the correlations between the 5-day-averaged fields are considerably lower (~0.3, Fig. 8e) than the correlations between SOSE and NCEP1 or SOSE and ERA, and they further drop in the vicinity of the ACC (~0.2). LY09 air–sea heat flux correlates better with the NCEP1 heat flux product (Figs. 8f), which can partly be attributed to the fact that LY09 used NCEP1 atmospheric fields as an initial guess. Whereas the correlations between ERA and ERA+C heat flux estimates were the highest among all the pairs of data considered, the correlations between NCEP1 and NCEP1+C are the lowest among all the data pairs. NCEP1+C correlation with SOSE is similarly very low.

5. Surface freshwater and buoyancy flux

The Southern Ocean is one of the most significant global regions of oceanic freshwater uptake, equaling or exceeding the high northern latitude uptake (e.g., Ganachaud and Wunsch 2003; Talley 2008). Although oceanic freshwater uptake is of fundamental importance for the density field, particularly at high latitudes, quantitative knowledge of air–sea freshwater fluxes is very limited because of the lack of reliable data for precipitation, evaporation, and terrestrial runoff (e.g., Trenberth et al. 2007). Even more so than for heat flux, freshwater flux estimates are very sparse and there is no acknowledged ''true'' baseline for evaporation minus precipitation ($E - P$) (Trenberth and Guillemot 1995).

In this section we show the time-averaged (years 2005–07) freshwater and buoyancy flux estimates for the six datasets (NCEP1, ERA, NCEP+C, and ERA+C SOSE, LY09), and we point out their major similarities and differences. The freshwater flux contribution to buoyancy flux is a function of surface salinity as well as of net $E - P$ [Eq. (1)]. Therefore a salinity dataset is required that is complementary to the $E - P$ dataset. Of the products that we consider, only SOSE has a salinity field. For the NCEP1, ERA, and LY09 buoyancy fluxes, sea surface salinity had to be obtained from a separate source. Sea surface salinity from the NCEP Global Ocean Data Assimilation System (GODAS; Behringer and Xue 2004) was combined with the NWP-based fluxes (NCEP1, ERA, and with-COARE fluxes) because GODAS uses momentum, heat, and freshwater flux from an NWP model (NCEP2) and is for this reason likely the most consistent available product for combination with the NWP-based fluxes. LY09 data were combined with sea surface salinity from the Polar Science Center Hydrographic Climatology (PHC2) [a blending of Levitus et al. (1998) and Steele et al. (2001) datasets], following Danabasoglu et al. (2009), because this was the salinity dataset used in the LY09 analysis (S. Griffies 2009, personal communication).

a. NCEP1 and ERA freshwater and buoyancy heat-equivalent flux

The quality of NCEP1 $E - P$ estimates has been questioned (Simmonds et al. 2005; Cullather et al. 1998; Genthon et al. 2003; LY09), because both E and P are derived solely from the model fields, without any constraining observations (Kalnay et al. 1996). The WGASF final report (Taylor 2000) shows that the NCEP1 precipitation estimates nevertheless closely resemble independent estimates between 50°S and 45°N. Farther poleward, all reanalyses considered by the WGASF (NCEP1, NCEP2, and ECMWF reanalysis ERA-15) show low correlations with the reference dataset [Climate Prediction Center (CPC) Merged Analysis of Precipitation (CMAP)—estimate by Xie and Arkin (1996, 1997)]. On the other hand, Smith et al. (2001) showed that the NCEP1 latent heat flux estimates over the ocean exceeded estimates derived from ship observations by 20 W m^{-2}, which is approximately equivalent to an uncertainty in evaporation of 60 cm yr^{-1}. The excess precipitation required to balance the excess evaporation in NCEP1, shown by Smith et al. (2001), occurs over land (WGASF).

The time-averaged (over years 2005–07) NCEP1 and ERA E-P estimates show the familiar pattern of net evaporation in subtropical gyres and net precipitation in the higher latitudes (Figs. 9a,b).

Compared with Q_{HF}, the magnitude of the Q_{FW} contribution to Q_{BF} [Eq. (2)] is small north of the ACC but significant poleward of the ACC (Figs. 1, 9, and 10). Over much of the region poleward of the ACC, Q_{HF} and Q_{FW} contributions to buoyancy flux tend to oppose each other for both NCEP1 and ERA.

NCEP1 shows higher evaporation in the subtropics and higher precipitation in the polar region than ERA (Fig. 11d).

b. SOSE and LY09 freshwater and buoyancy heat-equivalent flux

Relative to NCEP1, both LY09 and SOSE decrease net evaporation in the subtropics and net precipitation in the higher latitudes (Figs. 3d,e and 11e,b). The adjustments made by the two flux products are similar in both their large-scale pattern and amplitude, the adjustments differ most in the subtropical Pacific and Atlantic, where both LY09 and SOSE reduced the NCEP1

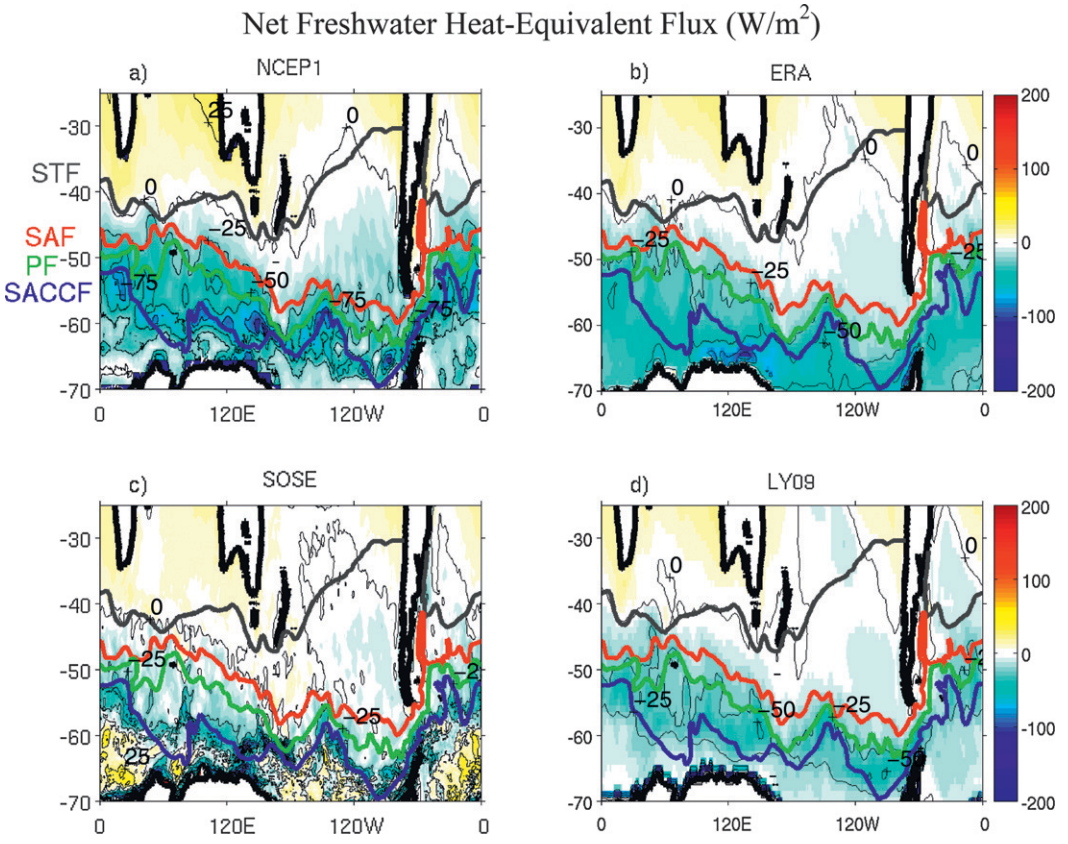

FIG. 9. As in Fig. 1, but for freshwater heat-equivalent flux given by Eq. (3) (W m^{-2}). Contour interval is 25 W m^{-2}. Colored lines as in Fig. 1.

net evaporation, but the SOSE adjustment was larger. The time-averaged SOSE freshwater heat-equivalent flux and buoyancy heat-equivalent flux (Figs. 9c and 10c) agree well with the LY09 fluxes (Figs. 9d and 10d) both in large-scale pattern and amplitude everywhere equatorward of the polar front.

c. *Correlations between 5-day-averaged E-P estimates*

Since precipitation is intermittent in space and time, the number of precipitation observations over the ocean is low, and evaporation estimates over the ocean have large uncertainties; $E - P$ estimates from various products are considerably more different and the correlations are lower than between the corresponding net air–sea heat flux estimates. Unlike the 5-day correlation between various air–sea heat flux estimates, where the largest correlations were between the two NWP model air–sea heat flux estimates (ERA and ERA+C as well as NCEP1 and ERA), the highest 5-day $E - P$ correlation is between SOSE and NCEP1 (Fig. 12b), indicating that although SOSE significantly changed NCEP1 $E - P$ during the optimization procedure, $E - P$ estimates between other pairs of products are even more different (Fig. 12). Although the large-scale pattern and magnitude of $E - P$ adjustment made by SOSE and LY09 were similar, the $E - P$ correlations between 5-day-averaged LY09 and SOSE $E - P$ estimates are very low (~0.1–0.3, Fig. 12d) and similar to the 5-day correlations between LY09 and NCEP1 (Fig. 12e).

6. Comparison of zonally averaged air–sea flux estimates

Zonal (ocean only) averages of the heat, freshwater, and buoyancy fluxes for each of the six products as a function of latitude (Fig. 13) are a useful way to summarize and visualize the differences between the various estimates that are intermediate between the full-scale maps of sections 4 and 5 and the mean differences averaged over all locations given in Table 4.

In the subtropics, equatorward of about 40°S, the net heat flux estimates differ in sign. It is expected that the ocean should be losing heat throughout the southern subtropics, which is a subduction region where surface

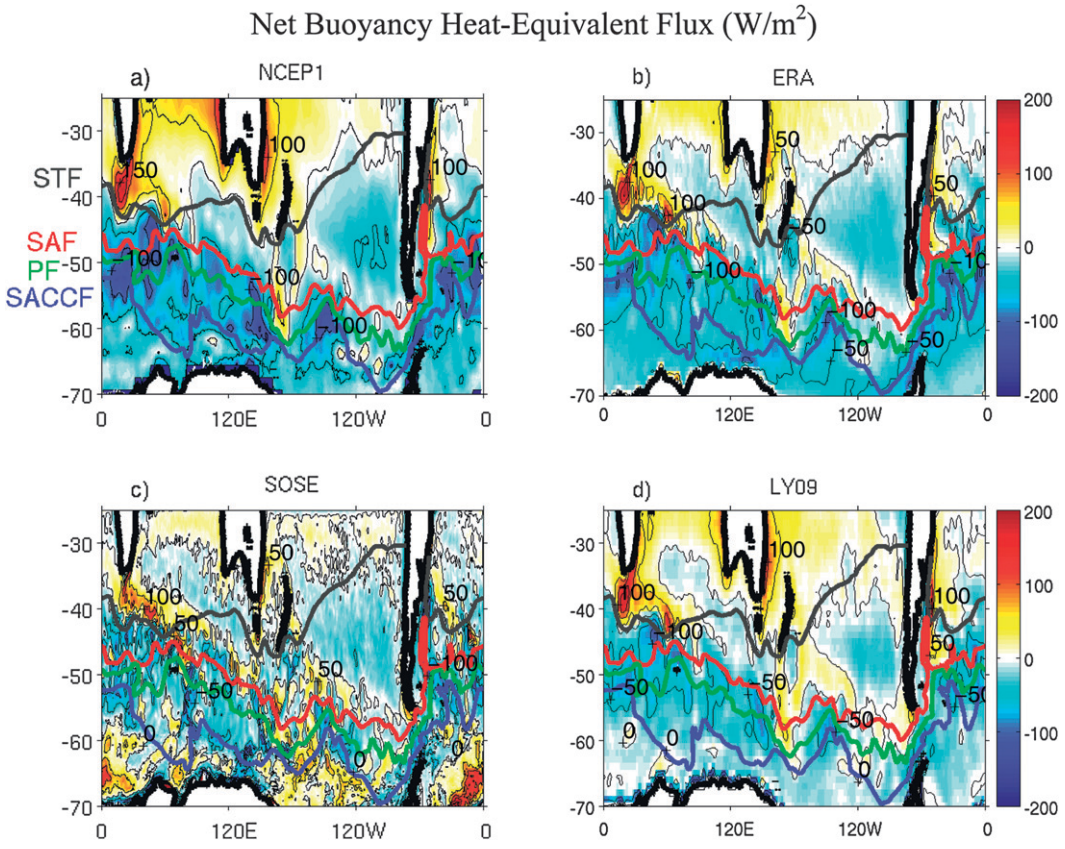

FIG. 10. As in Fig. 1, but for the buoyancy heat-equivalent flux from Eq. (2) (W m^{-2}), for example, the sum of the Figs. 1 and 9. Colored lines as in Fig. 1.

density, which is mostly governed by heat flux here, must increase. ERA, NCEP1, and LY09 show net ocean heat loss, and the zonally averaged SOSE fluxes are very close to zero, whereas ERA+C and especially NCEP1+C show unrealistic net ocean heat gain (Fig. 13a). The net evaporation in this latitude band (Fig. 13c) acts to decrease buoyancy (increase density) (Fig. 13e). Between about 40° and 60°S, net heating and freshwater input act together to increase buoyancy (reduce surface density) in all of the products. The heat and freshwater flux estimates differ most south of 60°S (Figs. 13b,d,f) since here the estimates are mostly numerical model results owing to the sparseness of observations (Kalnay et al. 1996; Röske 2006). South of about 60°S, freshwater input exceeds heat loss in all of the products except for SOSE, acting to increase buoyancy, which is inconsistent with our understanding of dense water formation in the highest latitudes of the Antarctic. In SOSE, cooling is larger than the freshwater input, and buoyancy is decreasing. This is probably because, of all of the products, SOSE must adjust the inputs to be consistent with the water mass properties, and therefore must generate a region of buoyancy decrease (density increase) in the far south.

The overall root-mean-square (RMS) differences between the net heat and freshwater heat-equivalent flux estimates, averaged over all time, longitudes, and ice-free regions in the latitude range 63.5°–25°S, are given in Table 4, along with the standard deviation of these differences. These overall values provide a condensed summary of the zonal time means of the RMS differences shown in the right-hand column of Fig. 13. Figure 3 showed that SOSE net air–sea heat flux adjustment of NCEP1 fields was larger than LY09 adjustment of NCEP1, whereas both SOSE and LY09 freshwater flux adjustments were similar. These are also illustrated by the RMS differences, as the RMS difference between SOSE and NCEP1 net air–sea flux is larger than the RMS difference between LY09 and NCEP1 net air–sea heat flux, while the RMS differences for freshwater heat-equivalent flux are similar. Thus, the SOSE and NCEP1 net air–sea heat flux difference is 30.9 ± 4.3 W m^{-2} and the LY09 and NCEP1 net air–sea heat flux difference is 22.3 ± 6.4 W m^{-2}; the SOSE and NCEP1 freshwater heat-equivalent

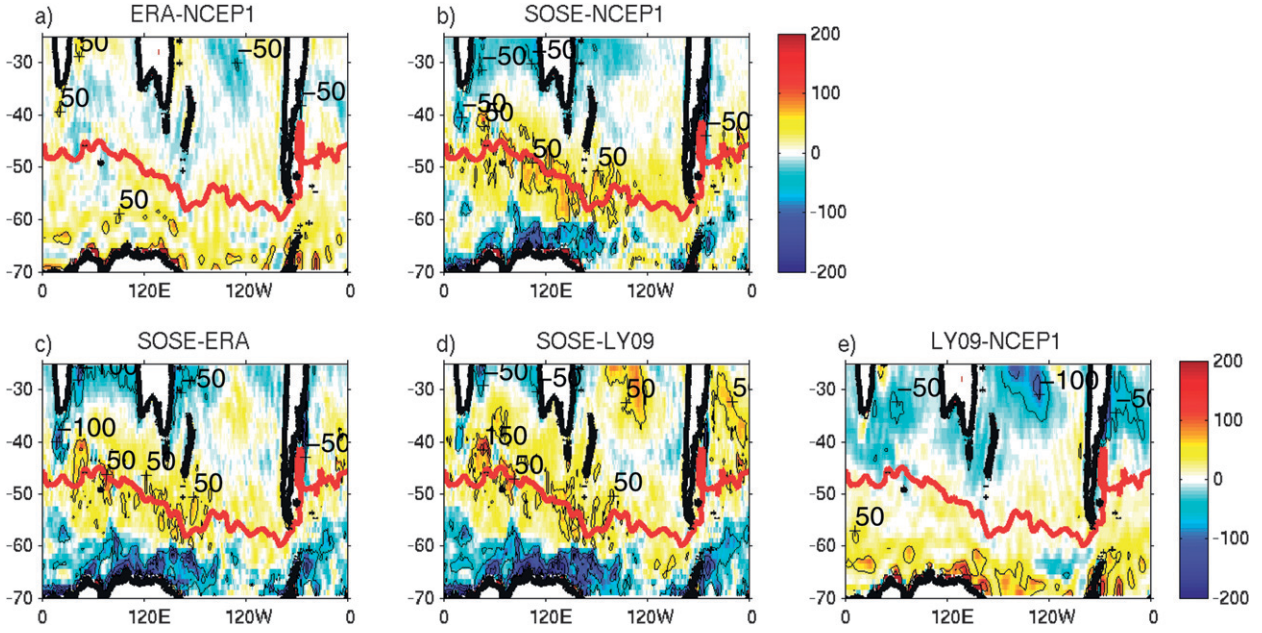

FIG. 11. Difference between time-averaged (years 2005–07) $E - P$ estimates interpolated on $1° \times 1°$ grid, contour interval 50 cm yr^{-1}. Titles identify source of $E - P$ estimates. Note different color scales for (a),(b), and (c)–(e). The red curve is the subantarctic front, as in Fig. 1.

flux difference is 12.8 ± 1.6 W m^{-2}, and the LY09 and NCEP1 freshwater heat-equivalent flux difference is 13.4 ± 0.9 W m^{-2}.

Both the NCEP1 and ERA heat flux products have a more ''balanced'' distribution of net heat flux out of the ocean in the subtropics and into the ocean in the higher latitudes than do the corresponding with-COARE flux estimates. LY09 shows a similar balance; SOSE on the other hand may be underestimating heat loss in the subtropics. That the with-COARE flux estimates show zonally averaged net ocean heat gain everywhere is unphysical, and is the main reason that

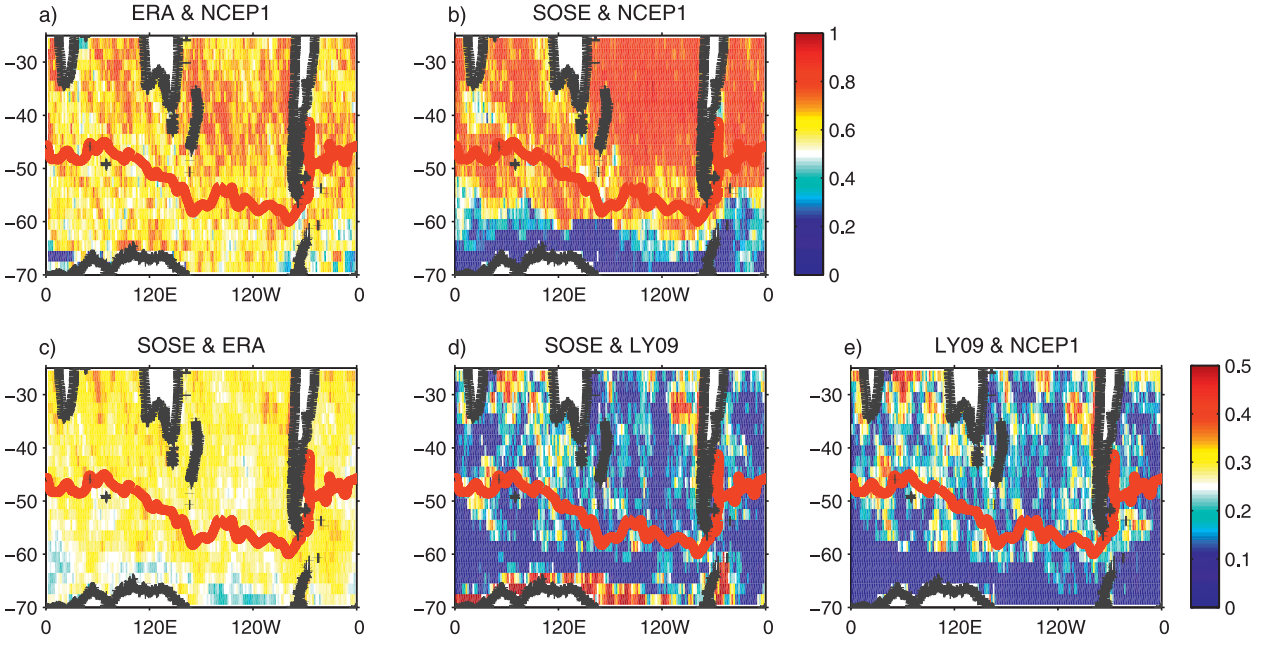

FIG. 12. A 3-yr average of correlation between 5-day anomalies of $E - P$ estimates shown in Fig. 11. The red curve is the subantarctic front, as in Fig. 1.

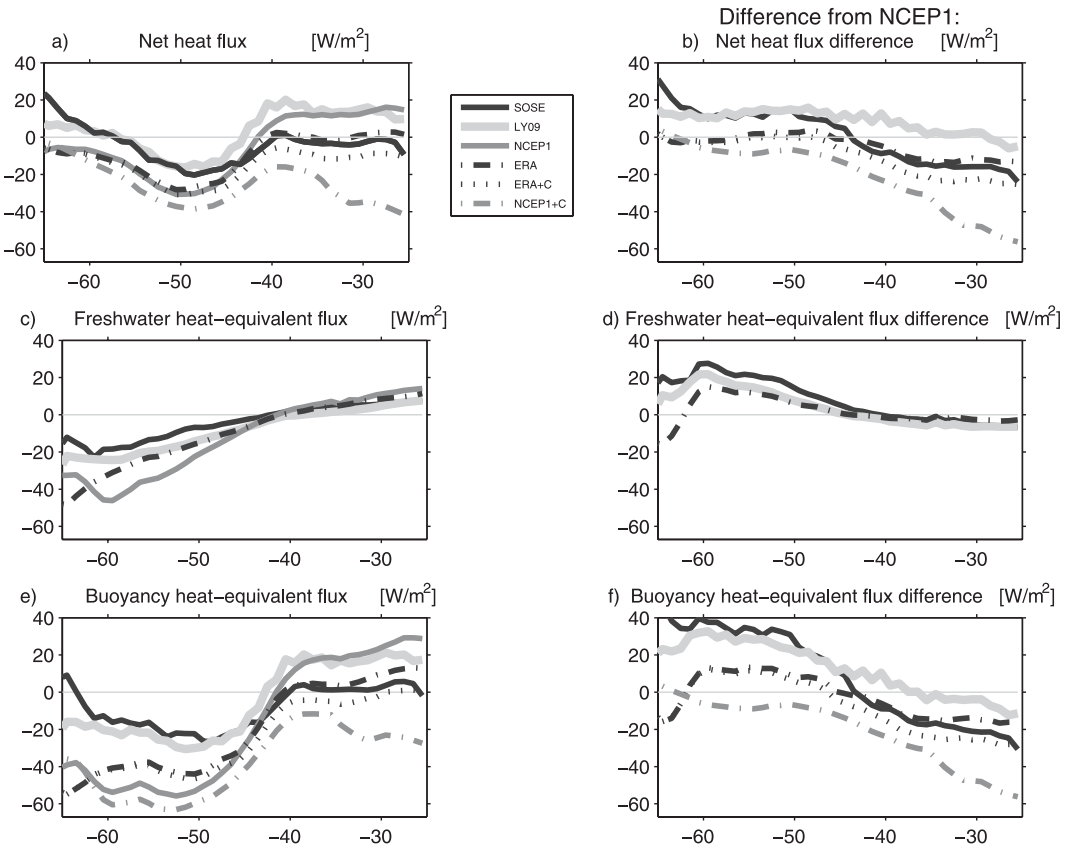

FIG. 13. Zonal and time (over years 2005–07) average of (a) net air–sea heat flux, (b) the difference between various net air–sea heat flux estimates and NCEP1 estimate, (c) freshwater heat-equivalent flux given by Eq. (3), (d) difference between freshwater heat-equivalent flux estimates and the NCEP1 freshwater heat-equivalent flux, (e) buoyancy heat-equivalent flux [sum of (a) and (c)], given by Eq. (2), and (f) difference between buoyancy heat-equivalent flux and NCEP1 buoyancy heat-equivalent flux, all for the six flux estimates considered in the text; the inset identifies source of flux estimate by line type. Positive (negative) values denote ocean buoyancy loss (gain) in all panels.

we recommend extreme caution in using with-COARE estimates in net buoyancy flux calculations that use unmodified radiation and freshwater flux fields from NCEP1/ERA. The COARE estimates might however be valid and useful when only the turbulent heat fluxes are of interest.

7. Discussion and conclusions

Air–sea flux estimates are especially poor in the Southern Ocean, largely because of the sparseness of both oceanic and meteorological ocean surface observations (e.g., Josey et al. 1999; Taylor 2000; Kubota et al. 2003;

TABLE 4. The RMS difference of monthly means and its standard deviation (years 2005–07) for net air–sea heat and freshwater heat-equivalent (boldface) flux estimates over the ocean south of 24.7°S. For the comparison all datasets are interpolated on a 1° × 1° grid. ''No FW'' means that there is no independent freshwater flux estimate.

	NCEP1	ERA	NCEP1+C	ERA+C	SOSE	LY09	
NCEP1	—	16.9 ± 2.6	35.3 ± 6.2	18.6 ± 3.0	30.9 ± 4.3	22.3 ± 6.4	RMS heat flux difference (W m^{-2})
ERA	**13.8 ± 2.4**	—	38.7 ± 6.1	4.8 ± 0.6	30.5 ± 5.1	24.4 ± 5.4	
NCEP1+C	**No FW**	**No FW**	—	37.5 ± 5.5	40.4 ± 5.5	37.6 ± 6.2	
ERA+C	**No FW**	**No FW**	**No FW**	—	30.3 ± 5.5	25.5 ± 5.4	
SOSE	**12.8 ± 1.6**	**13.8 ± 2.6**	**No FW**	**No FW**	—	33.8 ± 6.0	
LY09	**13.4 ± 0.9**	**12.3 ± 2.6**	**No FW**	**No FW**	**11.9 ± 1.2**	—	
RMS freshwater (heat-equivalent) flux difference (W m^{-2})							

Dong et al. 2007; M. Bourassa et al. 2011, personal communication). Accurate delineation of regions with buoyancy gain and loss is, however, of crucial importance for studies such as those of water-mass formation. Buoyancy fluxes in the Southern Ocean critically include freshwater fluxes as well as heat fluxes.

We have carried out an intercomparison of the following six surface buoyancy flux estimates, averaged over years 2005–07: two reanalyses (ERA and NCEP1), two recent flux products developed as an improvement of the NCEP1 (LY09 and SOSE), and two ad hoc air–sea flux estimates that are obtained by combining the NCEP1 or ERA net radiative fluxes with turbulent fluxes obtained using the COARE 3.0 bulk formulas with NCEP1 or ERA input variables. The intercomparison provides insight into the likely accuracy of the products in different regions.

Our principal focus is on the recently developed Southern Ocean State Estimate (SOSE). Although SOSE was not specifically designed to produce optimal air–sea flux fields, it does yield an adjusted set of such flux fields as a necessary by-product. Given the sparseness of the atmospheric observations needed to determine air–sea fluxes in the Southern Ocean, demonstrated improvement in flux accuracy through assimilation of oceanic observations in an ocean state estimate could be a very useful result. Our main results follow.

First, the SOSE adjustments of NCEP1 forcing fields (which SOSE used as an initial guess) largely correct the NCEP1 biases reported by WGASF, and they are largely in agreement with the independent adjustments of LY09. Since the methods and observations used by LY09 and SOSE to improve the NCEP1 atmospheric state estimate are very different, the good agreement between them lends a degree of confidence to both products.

The SOSE net air–sea flux estimates agree qualitatively well with the LY09 estimates in their large-scale pattern. The main difference is that overall SOSE estimates less ocean heat loss (more ocean heat gain) than LY09. The SOSE and LY09 turbulent heat flux adjustments are similar, whereas much smaller radiative heat flux adjustments differ. The main features in the large-scale pattern of LY09 and SOSE net air–sea heat flux differences relative to NCEP1 are increased ocean heat loss in the polar regions and predominantly decreased ocean heat loss in the subtropics and over the western boundary currents.

The large scale pattern of freshwater flux adjustments ($E - P$) made by SOSE and LY09 are very similar; relative to NCEP1, both decreased net evaporation in the subtropics (particularly in the South Pacific and Indian Oceans) and decreased net precipitation in the higher latitudes.

It is important to note that without comparison with observations we cannot fully assess the accuracy of SOSE fluxes and determine if SOSE fluxes represent a true improvement of NCEP1 initial guess. Nevertheless, the correlation coefficients and RMS differences between various datasets indicate that SOSE heat and freshwater flux estimates were consistent with the other commonly used flux estimates (NCEP1, ERA, LY09).

Second, even if SOSE net air–sea heat and freshwater fluxes were not a clear improvement of the initial NCEP1 fields, but only consistent with the other widely used products analyzed here, they are an important advance for the oceanographic studies such as, for example, the study of water-mass formation, which requires a complete and internally consistent set of surface flux fields and the three-dimensional oceanographic high-resolution fields that SOSE provides.

For studies that require only the sea surface oceanic data along with surface fluxes, SOSE still has an advantage over the NWP products as it provides sea surface temperature and salinity fields that are dynamically and thermodynamically consistent with the atmospheric forcing driving the SOSE ocean model. In contrast, when working with NWP model air–sea fluxes (such as NCEP1, ECMWF) and also LY09 flux estimates, to determine the surface density field, one needs to use sea surface salinity data from some other source. Considering that in the high latitudes of the Southern Ocean sea surface salinity plays an especially important role in determining the sea surface density, and that this is a region with sharp fronts and strong mesoscale activity, combining data from different sources may introduce inaccuracies.

Third, the net air–sea heat fluxes obtained by combining the NCEP1 or ERA net radiative flux with turbulent flux estimated using the COARE 3.0 bulk formulas with NCEP1 or ERA input fields were clearly unrealistic, yielding unbalanced net air–sea heat and buoyancy fluxes, with zonally integrated ocean heat gain at all latitudes south of 25°S. This however need not imply that the COARE 3.0 bulk formulas are inferior to those employed by NCEP1 and ERA, but rather suggests that COARE 3.0 latent and sensible heat flux estimates should not be combined with the unmodified radiative fluxes from the two NWP models (NCEP1 and ERA). The latter is supported by the results of Taylor (2000) and Weller et al. (2004) showing that biases in NCEP1 NSW and latent heat flux estimates tend to cancel, yielding a more balanced net air–sea heat flux estimate. Therefore, correcting only the NCEP1 latent heat flux bias (e.g., by using the COARE 3.0 bulk formulas) results in excess net ocean heat gain due to NSW bias.

Last, overall, the various air–sea buoyancy flux products differ most over the large ocean currents which have

strong, narrow fronts (e.g., the ACC and western boundary currents). Although this may not come as a surprise, it emphasizes the importance of allowing for a two-way atmosphere–ocean feedback and resolving mesoscale oceanic features.

The large differences between both heat and freshwater flux estimates by the six products considered here indicate that significant uncertainties remain, highlighting the need for high-quality in situ observations. Our results suggest that these observations need not be strictly of atmospheric variables. The ocean is an integrator of atmospheric fluxes, such that knowledge of the upper ocean heat and freshwater content, provided, for example, by Argo observations, places valuable constraints on the atmospheric state.

Meanwhile, planned improvements to SOSE include implementing a better set of constraints for the atmospheric state by using more accurate reanalysis products and also meteorological observations, in particular satellite-derived radiation estimates [e.g., the Moderate Resolution Imaging Spectroradiometer (MODIS) shortwave radiation; Pinker et al. (2009)]. There remains much work to do in accurately determining air–sea exchanges of heat and of freshwater in the Southern Ocean.

Acknowledgments. This work was supported by NSF Ocean Sciences Grants OCE-0327544, OCE-0850869 and OPP-0961218 to Scripps Institution of Oceanography. The work also benefited from support under NASA Grant EOS/03-0602-0117. Computational resources for SOSE were provided by NSF Teragrid resource Grant MCA06N007. NCEP Reanalysis data are provided by the NOAA/OAR/ ESRL PSD, Boulder, Colorado, from their web site at http://www.cdc.noaa.gov/. The ERA-Interim, GODAS, and LY09 (LY09 is listed as Coare2.0 Global air–sea flux dataset) data used in this study are from the Research Data Archive (RDA), which is maintained by the Computational and Information Systems Laboratory (CISL) at the National Center for Atmospheric Research (NCAR). NCAR is sponsored by the National Science Foundation (NSF). The original ERA-Interim data are available from the RDA (http://dss.ucar.edu) in dataset number ds627.0. The original LY09 data used here are available from the RDA (http://dss.ucar.edu) in dataset number ds260.2. The GODAS data are available from the RDA (http://dss.ucar.edu) in dataset number ds277.6. IC would like to thank Sarah Gille, Janet Sprintall, Steve Yeager, and especially Bill Large for motivating discussions as well as the three anonymous reviewers whose suggestions significantly improved this manuscript.

APPENDIX

Intercomparison of the Four NCEP1 and ERA Air–Sea Flux Components

Comparison of the individual air–sea heat flux components (NSW, NLW, latent heat flux, and sensible heat flux) estimated by NCEP1 and ERA does not reveal which dataset is more accurate, but it does provide a quantitative estimate of the discrepancy and uncertainty in these fields, although this estimate is likely a lower bound as errors common to both NWP model datasets cancel out. Comparison with NCEP1 biases estimated by the WGASF (Taylor 2000) provides information regarding whether any portion of the difference between the NCEP1 and ERA fields may be attributed to NCEP1 bias. (The WGASF did not analyze the ERA-Interim results.)

a. NSW and NLW radiation

The WGASF (Taylor 2000) showed that NCEP1 NSW radiation is biased low in the subtropics (shown as negative bias in Fig. 4d) and is biased high in the Drake Passage latitude band relative to the reference SRB dataset (Fig. 4c), with the strongest bias in subtropics. NCEP1 NSW radiation is less than ERA NSW radiation everywhere in the domain except in the southernmost part of the Southern Ocean (Fig. 4b), with the largest difference in the subtropics suggesting that at least a portion of the difference may be attributed to NCEP1 NSW radiation bias. NCEP1 and ERA NSW radiation differ less in the high latitudes.

The high-latitude NCEP1 NLW radiation is greater than ERA (Fig. 5b) and the SRB dataset, again suggesting a portion of the NCEP1 and ERA difference may be attributed to NCEP1 NLW bias. The net radiation estimated by the two NWP models (sum of NSW and NLW radiation) tends to be more similar than the individual radiation components. In the regions where ocean heat loss due to NCEP1 NLW radiation is smaller than ERA NLW radiation (e.g., in the subtropical eastern Indian Ocean and around Africa), NCEP1 NSW radiation heat gain is also less than ERA NSW radiation, so the biases tend to cancel.

b. Latent and sensible heat fluxes

NCEP1 and ERA latent heat flux estimates have very similar large-scale features, showing net ocean heat loss over almost the entire domain. ERA latent heat loss is greater almost everywhere (Fig. 6c), with the largest difference over the Agulhas retroflection region (partly on account of the higher resolution of ERA dataset) and

in the central subtropical Pacific and Atlantic. WGASF showed that in the Agulhas retroflection region, NCEP1 latent heat loss is biased low compared to the reference COADS dataset (Taylor 2000, their Fig. 11.4.2d reproduced as our Fig. 6d), which may explain part of the difference between NCEP1 and ERA in that region.

Similar to the latent heat flux fields, the large-scale features of NCEP1 and ERA sensible heat flux fields are consistent. They both show a net ocean heat loss almost everywhere, though the NCEP1 product does show a sensible heat gain poleward of the ACC (Fig. 7a,c). However, the WGASF assigns this to NCEP1 bias and suggests that NCEP1 sensible heat loss should be increased in many high latitude regions (poleward of about 55°S). NCEP1 sensible heat flux is greater than ERA heat flux in the subtropical Indian Ocean and western subtropical South Pacific and smaller elsewhere (Fig. 7c). The WGASF suggested, however, that NCEP1 sensible heat loss is an overestimate in many subtropical regions (Fig. 7d). This is in agreement with the results of Smith et al. (2001) who compared NCEP1 near-surface meteorological variables and air–sea flux fields to high-quality observations collected during the World Ocean Circulation Experiment (WOCE) and showed that NCEP sensible heat flux was too large.

REFERENCES

Behringer, D. W., and Y. Xue, 2004: Evaluation of the global ocean data assimilation system at NCEP: The Pacific Ocean. Preprints, *Eighth Symp. on Integrated Observing and Assimilation Systems for Atmosphere, Oceans, and Land Surface,* Seattle, WA, Amer. Meteor. Soc., 2.3. [Available online at http://ams.confex.com/ams/84Annual/techprogram/paper_70720.htm.]

Brunke, M. A., X. Zeng, and S. Anderson, 2002: Uncertainties in sea surface turbulent flux algorithms and datasets. *J. Geophys. Res.,* **107,** 3141, doi:10.1029/2001JC000992.

——, C. W. Fairall, X. Zeng, L. Eymard, and J. A. Curry, 2003: Which bulk aerodynamic algorithms are least problematic in computing ocean surface turbulent fluxes? *J. Climate,* **16,** 619–635.

Cai, W., B. Di, J. Church, T. Cowan, M. Dix, and L. Rotstayn, 2006: Pan-oceanic response to increasing anthropogenic aerosols: Impacts on the Southern Hemisphere oceanic circulation. *Geophys. Res. Lett.,* **33,** L21707, doi:10.1029/2006GL027513.

Campine, J. M., J. Marshall, and D. Ferreira, 2008: Sea ice-ocean coupling using a rescaled vertical coordinate *z**. *Ocean Modell.,* **24,** 1–14.

Chelton, D. B., M. G. Schlax, M. H. Freilich, and R. F. Milliff, 2004: Satellite measurements reveal persistent small-scale features in ocean winds. *Science,* **303,** 978–983.

Cullather, R. I., D. H. Bromwich, and M. L. VanWoert, 1998: Spatial and temporal variability of Antarctic precipitation from atmospheric methods. *J. Climate,* **11,** 334–367.

Curry, J. A., and Coauthors, 2004: SEAFLUX. *Bull. Amer. Meteor. Soc.,* **85,** 409–424.

Cusack, S., A. A. Slingo, J. M. Edwards, and M. Wild, 1998: The radiative impact of a simple aerosol climatology on the Hadley Centre atmospheric GCM. *Quart. J. Roy. Meteor. Soc.,* **124,** 2517–2526.

Danabasoglu, G., S. Peacock, K. Lindsay, and D. Tsumune, 2009: Sensitivity of CFC-11 uptake to physical initial conditions and interannually varying surface forcing in a global ocean model. *Ocean Modell.,* **29,** 58–65.

Darnell, W. L., W. F. Staylor, S. K. Gupta, N. A. Ritchey, and A. C. Wilber, 1992: Seasonal variation of surface radiation budget derived from International Satellite Cloud Climatology Project C1 Data. *J. Geophys. Res.,* **97,** 15 741–15 760.

da Silva, A. M., and G. White, 1996: Intercomparison of surface marine fluxes from GEOS-1/DAS and NCEP/NCAR reanalyses. *Proc. WCRP Workshop on Air–Sea Flux Fields for Forcing Ocean Models and Validating GCMs,* Reading, United Kingdom, WCRP Rep. WMO/TD-762, 19–24.

——, C. Young, and S. Levitus, 1994: *Atlas of Surface Marine Data 1994.* NOAA Atlas NESDIS, 5 volumes.

Dong, S., S. T. Gille, and J. Sprintall, 2007: An assessment of the Southern Ocean mixed layer heat budget. *J. Climate,* **20,** 4425–4442.

Fairall, C. W., E. F. Bradley, J. E. Hare, A. A. Grachev, and J. B. Edson, 2003: Bulk parameterization of air–sea fluxes: Updates and verification for the COARE algorithm. *J. Climate,* **16,** 571–591.

Forget, G., 2010: Mapping ocean observations in a dynamical framework: A 2004–06 ocean atlas. *J. Phys. Oceanogr.,* **40,** 1201–1221.

Ganachaud, A., and C. Wunsch, 2003: Large-scale ocean heat and freshwater transports during the World Ocean Circulation Experiment. *J. Climate,* **16,** 696–705.

Genthon, C., G. Krinner, and M. Sacchettini, 2003: Interannual Antarctic tropospheric circulation and precipitation variability. *Climate Dyn.,* **21,** 289–307.

Gill, A. E., 1982: *Atmosphere–Ocean Dynamics*. Academic Press, 662 pp.

Gulev, S. K., 1997: Climatologically significant effects of space–time averaging in the North Atlantic sea–air heat flux fields. *J. Climate,* **10,** 2743–2763.

——, 2003: Preface. *J. Climate,* **16,** 569.

——, T. Jung, and E. Ruprecht, 2007: Estimation of the impact of sampling errors in the VOS observations on air–sea fluxes. Part I: Uncertainties in climate means. *J. Climate,* **20,** 279–301.

Hibler, W. D., and K. Bryan, 1987: A diagnostic ice–ocean model. *J. Phys. Oceanogr.,* **17,** 987–1015.

Hines, K. M., D. H. Bromwich, and G. J. Marshall, 2000: Artificial surface pressure trends in the NCEP/NCAR reanalysis over the Southern Ocean and Antarctica. *J. Climate,* **13,** 3940–3952.

Hunke, E. C., 2001: Viscous–plastic sea ice dynamics with the EVP model: Linearization issues. *J. Comput. Phys.,* **170,** 18–38.

——, and J. K. Dukowicz, 1997: An elastic–viscous–plastic model for sea ice dynamics. *J. Phys. Oceanogr.,* **27,** 1849–1867.

Iudicone, D., G. Madec, B. Blanke, and S. Speich, 2008: The role of Southern Ocean surface forcings and mixing in the global conveyor. *J. Phys. Oceanogr.,* **38,** 1377–1400.

Josey, S., E. Kent, and P. Taylor, 1999: New insights into the ocean heat budget closure problem from analysis of the SOC air–sea flux climatology. *J. Climate,* **12,** 2856–2868.

Kalnay, E., and Coauthors, 1996: The NCEP/NCAR 40-Year Reanalysis Project. *Bull. Amer. Meteor. Soc.,* **77,** 437–471.

Karsten, R. H., and J. Marshall, 2002: Constructing the residual circulation of the ACC from observations. *J. Phys. Oceanogr.,* **32,** 3315–3327.

Kistler, R., and Coauthors, 2001: The NCEP/NCAR 50-Year Reanalysis Project: Monthly means CD-ROM and documentation. *Bull. Amer. Meteor. Soc.,* **82,** 247–267.

Klein, S. A., and D. L. Hartmann, 1993: The seasonal cycle of low stratiform clouds. *J. Climate,* **6,** 1587–1606.

Kubota, M., A. Kano, H. Muramatsu, and H. Tomita, 2003: Intercomparison of various surface latent heat flux fields. *J. Climate,* **16,** 670–678.

Large, W. G., and S. Pond, 1981: Open ocean momentum flux measurements in moderate to strong winds. *J. Phys. Oceanogr.,* **11,** 324–336.

——, and A. J. G. Nurser, 2001: Ocean surface water mass transformation. *Ocean Circulation and Climate,* G. Siedler et al., Eds., International Geophysics Series, Vol. 77, Academic Press, 317–336.

——, and S. G. Yeager, 2004: Diurnal to decadal global forcing for ocean and sea-ice models: The data sets and flux climatologies. NCAR Tech. Note NCAR/TN-460+STR, 105 pp.

——, and ——, 2009: The global climatology of an interannually varying air–sea flux data set. *Climate Dyn.,* **33,** 341–364.

Levitus, S., and Coauthors, 1998: *Introduction*. Vol. 1, *World Ocean Database 1998,* NOAA Atlas NESDIS 18, 346 pp.

Losch, M., D. Menmenlis, P. Heimbach, J.-M. Campin, and C. Hill, 2009: A dynamic-thermodynamic sea ice model on an Arakawa C grid for coupled ocean and sea ice state estimation. *EGU General Assembly 2009,* Vienna, Austria, EGU, Abstract EGU2009-9194.

Mazloff, M. R., P. Heimbach, and C. Wunsch, 2010: An eddy-permitting Southern Ocean state estimate. *J. Phys. Oceanogr.,* **40,** 880–899.

Moore, G. W. K., and I. A. Renfrew, 2002: An assessment of the surface turbulent heat fluxes from the NCEP reanalysis over western boundary currents. *J. Climate,* **15,** 2020–2037.

O'Neill, L. W., D. B. Chelton, S. K. Esbensen, and F. J. Wentz, 2005: High-resolution satellite observations of SST modification of the marine atmospheric boundary layer over the Agulhas Return Current. *J. Climate,* **18,** 2706–2723.

Orsi, A. H., T. Whitworth III, and W. D. Nowlin Jr., 1995: On the meridional extent and fronts of the Antarctic Circumpolar Current. *Deep-Sea Res.,* **42,** 641–673.

Pinker, R. T., H. Wang, and S. A. Grodsky, 2009: How good are ocean buoy observations of radiative fluxes? *Geophys. Res. Lett.,* **36,** L10811, doi:10.1029/2009GL037840.

Renfrew, I. A., G. W. K. Moore, P. S. Guest, and K. Bumke, 2002: A comparison of surface-layer and surface turbulent-flux observations over the Labrador Sea with ECMWF analyses and NCEP reanalyses. *J. Phys. Oceanogr.,* **32,** 383–400.

Reynolds, R. W., and T. M. Smith, 1994: Improved global sea surface temperature analyses using optimum interpolation. *J. Climate,* **7,** 929–948.

——, and ——, 1995: A high-resolution global sea surface temperature climatology. *J. Climate,* **8,** 1571–1583.

Röske, F., 2006: A global heat and freshwater forcing dataset for ocean models. *Ocean Modell.,* **11,** 235–297.

Scott, J. D., and M. A. Alexander, 1999: Net shortwave fluxes over the ocean. *J. Phys. Oceanogr.,* **29,** 3167–3174.

Siefridt, L., B. Barnier, K. Béranger, and H. Roquet, 1999: Evaluation of operational ECMWF surface heat fluxes: Impact of parameterisation changes during 1986–1995. *J. Mar. Syst.,* **19,** 113–135.

Simmonds, I., and M. Dix, 1989: The use of mean atmospheric parameters in the calculation of modeled mean surface heat fluxes over the world's oceans. *J. Phys. Oceanogr.,* **19,** 205–215.

——, and W. F. Budd, 1991: Sensitivity of the Southern Hemisphere circulation to leads in the Antarctic pack ice. *Quart. J. Roy. Meteor. Soc.,* **117,** 1003–1024, doi:10.1002/qj.49711750107.

——, A. S. Rafter, T. D. Cowan, A. B. Watkins, and K. Keay, 2005: Large-scale vertical momentum, kinetic energy and moisture fluxes in the Antarctic sea-ice region. *Bound.-Layer Meteor.,* **117,** 149–177.

Simmons, A., S. Uppala, D. Dee, and S. Kobayashi, 2006: ERA-Interim: New ECMWF reanalysis products from 1989 onwards. *ECMWF Newsletter,* No. 110, ECMWF, Reading, United Kingdom, 25–35.

Smith, S. R., D. M. Legler, and K. V. Verzone, 2001: Quantifying uncertainties in NCEP reanalyses using high-quality research vessel observations. *J. Climate,* **14,** 4062–4072.

Speer, K., S. R. Rintoul, and B. Sloyan, 2000: The diabatic Deacon cell. *J. Phys. Oceanogr.,* **30,** 3212–3222.

Stammer, D., and Coauthors, 2002: Global ocean circulation during 1992–1997, estimated from ocean observations and a general circulation model. *J. Geophys. Res.,* **107,** 3118, doi:10.1029/2001JC000888.

——, K. Ueyoshi, A. Kohl, W. G. Large, S. A. Josey, and C. Wunsch, 2004: Estimating air–sea fluxes of heat, freshwater, and momentum through global ocean data assimilation. *J. Geophys. Res.,* **109,** C05023, doi:10.1029/2003JC002082.

Steele, M., R. Morley, and W. Ermold, 2001: PHC: A global ocean hydrography with a high quality Arctic Ocean. *J. Climate,* **14,** 2079–2087.

Talley, L. D., 2008: Freshwater transport estimates and the global overturning circulation: Shallow, deep and throughflow components. *Prog. Oceanogr.,* **78,** 257–303, doi:10.1016/j.pocean.2008.05.001.

Taylor, P. K., Ed., 2000: Intercomparison and validation of ocean-atmosphere energy flux fields—Final report of the Joint WCRP/SCOR Working Group on Air–Sea Fluxes. WMO Rep. WCRP-112, WMO/TD-1036, 306 pp. [Available online at http://www.noc.soton.ac.uk/ooc/WGASF/.]

Thiebaux, J., E. Rogers, W. Wang, and B. Katz, 2003: A new high-resolution blended real-time global sea surface temperature analysis. *Bull. Amer. Meteor. Soc.,* **84,** 645–656.

Trenberth, K. E., and C. J. Guillemot, 1995: Evaluation of the global atmospheric moisture budget as seen from analyses. *J. Climate,* **8,** 2255–2272.

——, and Coauthors, 2007: Observations: Surface and atmospheric climate change. *Climate Change 2007: The Physical Science Basis,* S. Solomon et al., Eds., Cambridge University Press, 235–336.

Vianna, M. L., V. V. Menzies, A. B. Pezza, and I. Simmonds, 2010: Interactions between Hurricane Catarina (2004) and warm core rings in the South Atlantic Ocean. *J. Geophys. Res.,* **115,** C07002, doi:10.1029/2009JC005974.

Walin, G., 1982: On the relation between sea surface heat flow and thermal circulation in the ocean. *Tellus,* **34,** 187–195.

Warren, B. A., J. H. LaCasce, and P. E. Robbins, 1996: On the obscurantist physics of ''form drag'' in theorizing about the Circumpolar Current. *J. Phys. Oceanogr.,* **26,** 2297–2301.

Weller, R. A., F. Bradley, and R. Lukas, 2004: The interface or air–sea flux component of the TOGA Coupled Ocean–Atmosphere Response Experiment and its impact on subsequent air–sea interaction studies. *J. Atmos. Oceanic Technol.,* **21,** 223–257.

White, G., Ed., 1996: WCRP workshop on air–sea flux fields for forcing ocean models and validating GCMs. World Meteorological Organization Rep. WCRP 201395, WMO/TD Rep. 762, 184 pp.

Wild, M., 1999: Discrepancy between model-calculated and observed atmospheric shortwave absorption in areas with high aerosol loadings. *J. Geophys. Res.,* **104** (D22), 27 361–27 371.

——, 2005: Solar radiation budgets in atmospheric model intercomparisons from a surface perspective. *Geophys. Res. Lett.,* **32,** L07704, doi:10.1029/2005GL022421.

Xie, P., and P. A. Arkin, 1996: Analyses of global monthly precipitation using gauge observations, satellite estimates, and numerical model predictions. *J. Climate,* **9,** 840–858.

——, and ——, 1997: Global precipitation: A 17-year monthly analysis based on gauge observations, satellite estimates, and numerical model outputs. *Bull. Amer. Meteor. Soc.,* **78,** 2539–2558.

Yu, L., and R. A. Weller, 2007: Objectively analyzed air–sea heat fluxes for the global ice-free oceans (1981–2005). *Bull. Amer. Meteor. Soc.,* **88,** 527–539.

Zhang, Y.-C., W. B. Rossow, A. A. Lacis, V. Oinas, and M. I. Mishchenko, 2004: Calculation of radiative fluxes from the surface to top of atmosphere based on ISCCP and other global data sets: Refinements of the radiative transfer model and the input data. *J. Geophys. Res.,* **109,** D19105, doi:10.1029/2003JD004457.